SELF-POWERED FLEXIBLE ELECTROMECHANICAL SENSORS FOR PERSONAL HEALTH EVALUATION

by

WEI ZHAOLIN **LING ZHIJIE**

B.Sc. in Electromechanical Engineering

2023/2024

Faculty of Science and Technology
University of Macau

Self-powered Flexible Electromechanical Sensors for Personal Health Evaluation

WEI ZHAOLIN (DC027914)

LING ZHIJIE (DC028380)

Final Year Project Report submitted in partial fulfilment of the requirements for the degree of

BSc. in Electromechanical Engineering

Faculty of Science and Technology
University of Macau

2023/2024

University of Macau

Abstract

SELF-POWERED FLEXIBLE ELECTROMECHANICAL SENSORS FOR PERSONAL HEALTH EVALUATION

Wei Zhaolin (DC027914)

Ling Zhijie (DC028380)

Project Supervisor
Assistant Professor, Zhong Junwen

Self-powered Flexible Electromechanical Sensors for Personal Health Evaluation

Sleep apnea is a common disorder that seriously affects the quality of sleep and daily life. Since traditional methods are expensive, complex, and inconvenient, developing lightweight, low-power sleep apnea detection systems is crucial for user sleep monitoring technologies. Wearable devices are one solution, and we designed a flexible sandwich-structured pressure sensor that utilises piezoelectret materials and a comfortable human-computer interface to detect tiny pulse vibrations. The sensor adopts an optimized parallel capacitance structure, with conductive silver electrodes coated on the surface of the FEP film on both sides of a 4×4 cm^2 ultrathin piezoelectret device. Experiments show that the sensor has excellent charge decay retention and can be self-powered. We bonded the four corners of the FEP film with double-sided tape to create a cavity inside the ultrathin sensor structure. This resulted in a total sensor thickness of about 300 μm and improved sensitivity. On the other hand, the sleep heartbeat monitoring system consists of a self-powered pressure sensor, an Arduino-based circuit board, and a power supply. For signal processing and classification, we attempted to provide an end-to-end solution for ECG recognition using deep learning, thus eliminating the need for manual filtering and feature extraction. We have combined Convolutional Neural Network (CNN) network architecture with Recurrent Neural Networks (RNN) to achieve high accuracy in a 5-level classification task.

Keywords: Electrocardiogram, Sleep Apnea, Convolutional Neural Network, Soft Sensor, Fluorinated Ethylene Propylene

TABLE OF CONTENTS

LIST OF FIGURES

LIST OF TABLES

LIST OF ABBREVIATIONS

Abbreviation. CNN: Convolutional Neural Network

Abbreviation. ECG: Electrocardiograph

Abbreviation. FEP: Fluorinated Ethylene Propylene

Abbreviation. OSA: Obstructive Sleep Apnea

Abbreviation. PET: Polyethylene Terephthalate

Abbreviation. PSG: Polysomnography

Abbreviation. SAS: Sleep Apnea Syndrome

Abbreviation. SCA: Sudden Cardiac Arrest

Abbreviation. SCD: Sudden Cardiac Death

Abbreviation. SFS: Self-powered Flexible Sensor

ACKNOWLEDGEMENTS

The acknowledgements are often the last part to write. It was not until I reached this point that I felt the imminent end of my undergraduate studies. Stumbling through this journey, choosing the path I wanted and becoming the person I once dreamed of, would have been impossible without the help and support of my family, teachers, friends, and classmates.

First and foremost, I want to thank my family. From them, I've learned much about optimism, bravery, sincerity, kindness, effort, and perseverance. Their love for me and their unconditional trust and support have made me a braver and more compassionate person. Sometimes, when I feel down or unhappy, I opt to make a video call home to see the changes around me. Each video call recharges my batteries. I keep many photos of my younger sister on my phone, and when I'm feeling stressed, I look at those photos and videos. Becoming a big brother has made me feel more responsible and motivated to change the future for my family.

I am extremely lucky to have met some very good friends in my life. I would especially like to thank Tianjun Lan, Junjie Gao, Yifei Huang, Xianshu Lu, Yihan Chen, Dechao Jiang, Tong Zhang, Qilin Sun, Xiaoshi Ji, Minxing Huang, Xinyu Wang, Zijun Zhou, Zhijie Ling, Zhongxian Mai, Yubo Cui, Zhengchen Liu and Weijie Han. They have supported me through tough times and cheered for me in moments of joy. Friends are the family we choose, and I am so fortunate to have met them. I love you all.

I started learning music before I was even five years old, and since then, music has been an inseparable part of my life. While loneliness can be unbearable for many, for me, listening to classical music feels like conversing with the pioneers of music. Beethoven holds the highest place in my heart, and I am immensely grateful for his inspiring compositions. I always draw strength from his symphonies and sonatas. His longing for freedom and equality also resonates with me. Music has also brought more people into my life, and I thank the conductors Leung Kin Hang and Ng Sa from the UM

Symphonic Band for allowing me to learn the Bassoon and for the enriching stage experiences and friendships I gained there.

President Mei Yiqi of Tsinghua University once said, "The term 'university' does not refer to having grand buildings, but to having great scholars." The caliber of professors is often a critical measure of a university's strength. I am grateful to have met a group of excellent professors at the University of Macau, especially professors Junwen Zhong, Iekman Lei, Yan Su, Kinho Lo, and Puiin Mak for their tolerance, support, and encouragement. I would also like to express my gratitude to the doctoral student Xiao Guan and Dazhe Zhao at Professor Junwen Zhong's lab.

There are many more people I would like to thank for my four years of university life, but space is limited, and I cannot list them all. I still want to say thank you.

Wei Zhaolin

In my graduation design, the first thing I would like to thank is the people who helped guide us in this: the tutor, Professor Zhong Junwen, as well as the doctoral students who helped us, Zhao Dazhe, Guan Xiao and so on. When we encountered some difficult problems, they gave guidance direction, including the design of our device's back-end arduino platform to provide hardware help. I would like to express my heartfelt thanks to my partner, Wei Zhaolin, who pushed me throughout the whole design process to make me work more efficiently, he also took on a lot of tasks himself while completing the whole project very well, and I have learnt a lot from him.

Secondly, I would like to thank my family, they gave me a lot of encouragement and help during my senior year, they travelled thousands of miles from home to take care of me when I was sick, guided me when I was lost, and spurred me on when I was lazy. Especially my mother, who was in touch with me on phone from time to time, gave me love and care, financial support and taught me to be strong and serious about my predicament.

I would like to thank my best classmates and friends in the EME department, Dechao Jiang, Junjie Gao, Tong Zhang, Xianshu Lu, Yifei Huang, Yihan Chen, Zhaolin Wei,

Xi Chen, Zihao Wnag, Qilin Sun, Hengbo Li, Ian Lao, Judong Liu. Ian Lao, Judong Liu, etc., for their care and encouragement, and for accompanying me through the 4 years, with them, I never feel alone.

Then I would like to thank all the professors who teach in our EME department, especially: Professor Vai Kuong SIN for his kind words; Professor Kin Ho LO for his meticulous and friendly teaching; Professor Yan SU for his grounded lectures and so on. From them, I can feel their concern and warm hope for our future.

Participating in football activities is a stopover in my study life, and when I am not thinking about being idle, playing a game of football can revive my spirit. I would like to give special thanks to Xinyu Wang, Zijun Zhou, Zhongxian Mai and also Zhaolin Wei, who are my best mates on the pitch and motivators in my studies, and I am very grateful to them for their care and motivation.

I would also like to thank my AUC mates who laughed and played with me and those who have not yet graduated: Shaofeng Xu, Cefang Deng, Zihao He, Yi Pan, Zeibing Wang, Jiangjun Liang, Zhiyuan Wen and others, with whom the time I spent with has helped to alleviate the pain of adversity and inspired me to grow. I would also like to thank my books.

I would also like to thank my college, CKYC, for giving me a warm home for four years. The tutors, staff, and students were all very friendly and helped me when I encountered scams, which always warmed my heart.

Ling Zhijie

CHAPTER 1: INTRODUCTION

1.1 BACKGROUND

One-third of a person's life is spent in sleep, sleep apnea and sleep arrhythmia will reduce patients' sleep quality and quality of life significantly, and some subsequent complications will also make their diseases of the cardiovascular system significantly. Based on the findings of the National Commission on Sleep Disorders Research, an estimated annual total of 38,000 deaths are attributed to cardiovascular issues that are in some way associated with sleep apnea. Therefore, early identification of the disease is essential. According to the current epidemiological survey preliminary statistics, the incidence of Obstructive Sleep Apnea (OSA) in China is 2% to 4%, and the affected population is about 176 million. Therefore, for such a high incidence, it is necessary to make an early diagnosis[1].

Despite significant advances in cardiovascular medicine, sudden cardiac death (SCD) remains a serious medical and societal challenge, with millions of people dying each year from SCD. At the same time, it was noted that despite the technological and medical advances of the 21st century, the survival rate from sudden cardiac arrest (SCA) remains unacceptably low at less than 10 per cent in most parts of the world. If it occurs during sleep, there is a lower survival rate[2].

The routine diagnosis of OSA is based on the polysomnography (PSG) results. This test requires the patient to sleep for the whole night in the sleep monitoring laboratory of the hospital, and the polysomnographic signals are recorded to clarify whether the patient

has sleep apnea during this period and whether the diagnosis of OSA is established. The popularity of polysomnography is relatively low due to the high cost of the equipment and the high space requirements[3]. However, various screening methods (e.g., questionnaire screening, portable sleep monitor screening, etc.) have been used in the clinic, which can make up for this deficiency to a certain extent. Portable sleep monitoring and screening devices do not have the cumbersome requirements of polysomnography devices and monitor only a few simple signals, such as oro-nasal airflow and pulse signals. As a result, patients can then take the portable device home for monitoring, and the collected signals can be analysed the next morning to assess their likelihood of having OSA. These initial screening methods make early diagnosis of sleep apnea easier.

1.2 Fundamental Knowledge of Obstructive Sleep Apnea and Electrocardiogram Signals

Sleep Apnea Syndrome (SAS) is a potentially lethal sleep-breathing disease. Respiratory exercise affects the electrophysiological activity of cardiac myocytes in the heart, leading to changes in the electrocardiographic waveform. The waveform feature information extracted from the ECG signal can be used as a feature to characterise SAS. Therefore, ECG signals are the most used physiological signals in the study of automated SAS detection. This chapter serves as preparatory knowledge, starting with a brief overview of the pathogenesis of SAS and the basics of ECG. SAS severity levels are classified according to Table S1.

1.2.1 Pathogenesis of Obstructive Sleep Apnea

The main causes of OSA are as follows: Firstly, the anatomical structure of the upper airway is abnormal, leading to different degrees of airway narrowing and obstruction; secondly, the upper airway dilatation muscle tension is abnormal; thirdly, the mucous oedema of the upper airway tissues, body. Thirdly, mucous oedema of upper respiratory tract tissues, obesity, enlarged tonsils and pharyngeal tumors can also cause OSA.

In the case of apnea due to blockage of the upper respiratory tract for the reasons mentioned above, the respiratory center of the brain continues to send out respiratory impulses to elicit respiratory muscle excitation, so that respiration of the thorax and abdomen still exists[4]. Still, the airway is not flushed open as a result. With the prolongation of apnea, the carbon dioxide level in the body continues to rise, the stimulation of the respiratory center is enhanced, and the thoracic and abdominal part of the respiratory movement is very violent, leading to the sudden awakening of the person. Upon awakening the upper airway opens and airflow returns to normal.

1.2.2 Normal ECG Manifestations

The ECG signal is a weak, periodic, nonlinear time-varying physiological electrical signal, one of the most important physiological electrical signals in the human body, with a frequency range of 0.05~100 Hz. It is one of the most important physiological electrical signals in the human body. ECG signals are collected in a non-invasive way, i.e., by placing measurement electrodes on specific parts of the human body surface. The ECG signal is acquired in a non-invasive way, i.e., by placing measurement

electrodes on a specific part of the human body surface and recording the change of the potential difference during the cardiac activity[5]. As shown in Figure 1.1, the normal ECG signal activity cycle consists of P-wave, QRS wave group, T-wave, and U-wave, and can also be divided into S-T segments, At the same time, it can also be divided into different intervals such as S-T segment, PR interval, QT interval.

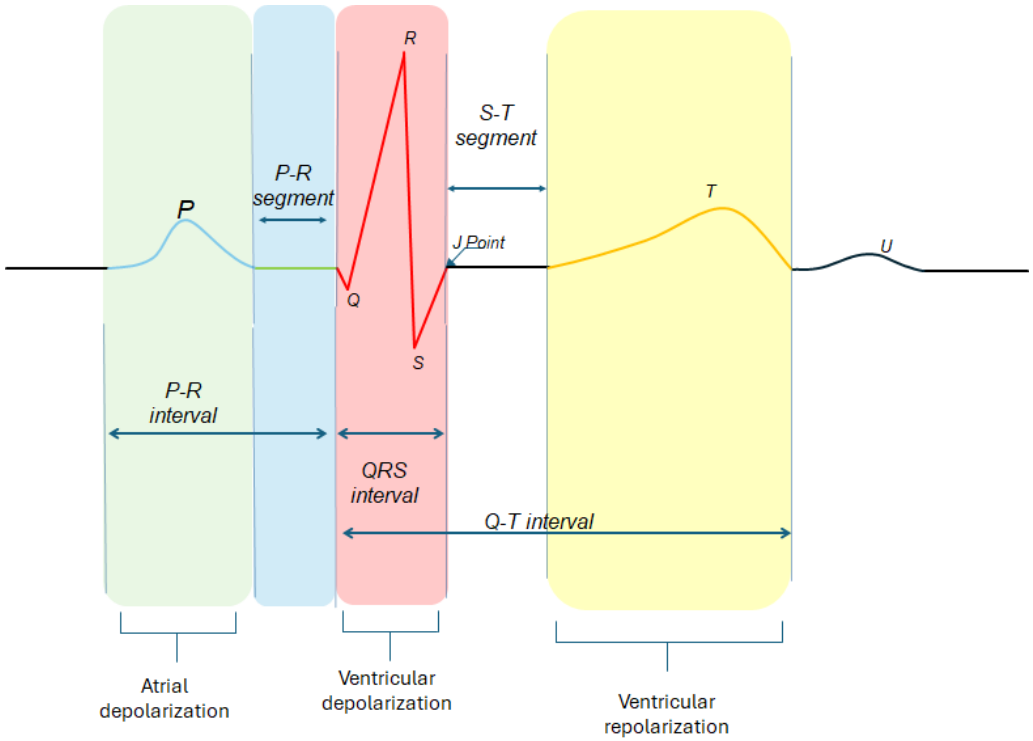

Figure 1.1 Typical ECG signal waveform

Each waveform and interval in the ECG signal have a different physiological significance and all are of medical research value[6].

P-wave: the first waveform of each cycle of the ECG signal, representing the potential changes generated during atrial depolarisation.

PR interval: the interval from the starting point of the P wave to the starting point of the QRS wave cluster, indicating the total duration of depolarisation from the beginning of atrial depolarisation to the beginning of ventricular depolarisation.

QRS wave group: It consists of Q wave, R wave, and S wave, and indicates the potential changes generated during the depolarisation of the two ventricles; Q wave is directed downward and has a small amplitude. Q wave is directed downward with a small amplitude, usually around 0.1 mV; R wave is directed upward and is the most obvious and largest amplitude wave in the whole ECG signal cycle. The R wave is the most obvious and largest in the whole ECG signal cycle, generally between 0.5 and 1.5 mV; the S wave is downward, generally around 0.2 mV. The duration of a typical QRS wave group is between 0.06 and 0.10 s. If the duration is longer than that, it may be because the QRS is not working. If this period is exceeded, it may be due to ventricular hypertrophy or intraventricular block. If this period is exceeded, it may be due to ventricular hypertrophy or intraventricular block.

The S-T segment: The interval from the end of the QRS wave group to the beginning of the T wave indicates that the ventricles are depolarising and have not yet entered the repolarisation state. There is no potential difference, and it is generally flush with the baseline. The duration of the S-T segment is generally between 0.05 and 0.15 s.

T-wave: T-wave appears after the S-wave and the direction is upward, indicating the potential change generated during the repolarisation of the two ventricles. The duration of the T-wave is usually between 0.15 and 0.25 s.

QT interval: The interval from the beginning of the QRS wave group to the end of the T wave, indicating the total time required for the completion of depolarization and repolarization of the two ventricles, generally between 0.36 and 0.44 s. In clinical practice, the length of the QT interval can be used to diagnose ventricular fibrillation, ventricular fibrillation, and ventricular fibrillation.

U-wave: U-wave appears after T-wave, and its direction is the same as that of T-wave, which is generally related to ventricular repolarization.

RR interval: the spacing of R waves between two adjacent ECG signal cycles, generally between 0.8 and 1.0 s in duration.

The RR interval is inversely proportional to the heart rate, the faster the heart rate, the shorter the RR interval, which is an important indicator to reflect the state of the heart.

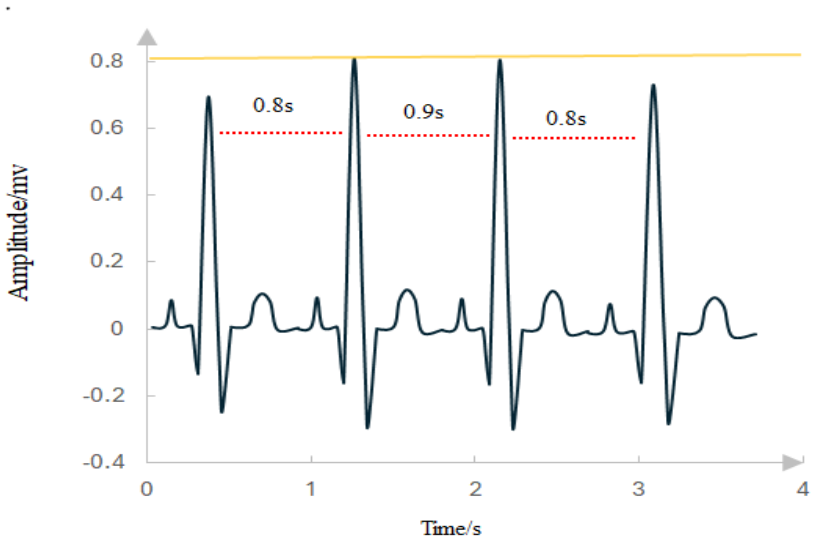

Figure 1.2 Fragments of ECG signals during normal respiration

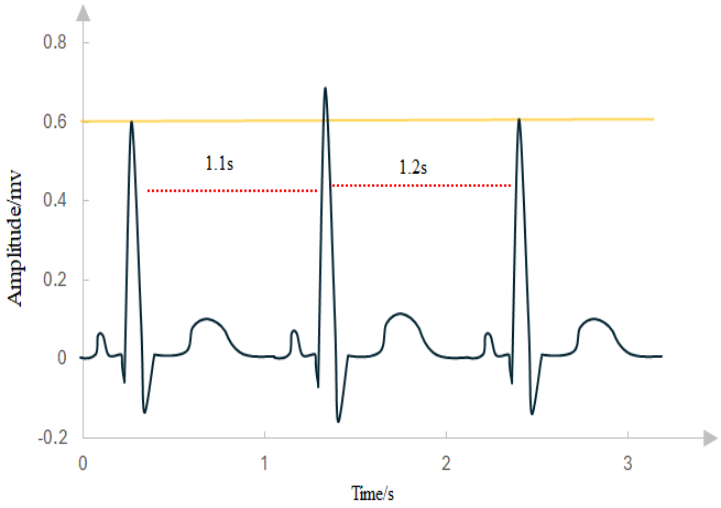

Figure 1.3 Fragments of ECG signals during apnea

A comparison of the changes in ECG signals during normal breathing and in sleep apnea is shown in Figure 1.2 and Figure 1.3. The RR intervals of the ECG signals during normal breathing were mainly between 0.8 and 1.0 s, and the R-wave amplitudes were mainly between 0.6 and 0.8 mV. The RR interval of the ECG signals

during sleep apnea was mainly between 1.1 and 1.2 s, which was greater than the RR interval of the ECG signals during normal respiration, and the R-wave amplitude mainly fluctuated between 0.6 and 0.6 mV, which was lower than the R-wave amplitude of the ECG signals during normal respiration. The R-wave amplitude mainly fluctuates around 0.6 mV, which is lower than the R-wave amplitude of normal respiration.

1.3 Structure of the Report

This report focuses on sleep health evaluation. For the current problem of high computational complexity and high overhead, a set of lightweight self-powered hardware designs and sleep apnea-arrhythmia detection algorithms based on ECG signals are proposed.

The main contents of the chapters of this paper are as follows:

Chapter 1 mainly introduces the basic knowledge of ECG signals and research significance.

Chapter 1 is about our research topic, briefly in this chapter we discuss the background of our research: the prevalence and impact of sleep apnea, the limitations of traditional diagnostic methods, and the need for lightweight, low-power sleep apnea detection systems for wearable devices.

Chapter 2 is a literature review divided into two sections on the current state of research in hardware and machine learning signal processing. The hardware section covers the development and status of flexible self-powered sensors for health monitoring, as well as challenges in output enhancement, stability and integration. Various signal

processing techniques for QRS detection and sleep apnea classification are also presented.

Chapter 3 describes our experimental design process, starting with the design of the flexible pressure sensor, covering mainly why piezoelectric materials such as Fluorinated Ethylene Propylene (FEP) and silver electrodes were used to create sandwich-structured sensors with optimised parallel capacitor configurations. The working mechanism of the sensor, the integration of the electrical system with the Arduino board and power supply, and the deep learning model used for ECG recognition, including data acquisition, pre-processing, R-wave detection, and feature extraction using a convolutional neural network (CNN), are also described.

Chapter 4 deals with the results and discussion of our research, focusing on sensor performance evaluation and algorithm validation, including durability and reliability tests, pressure sensitivity tests and step-input tests to evaluate dynamic characteristics, as well as experiments with volunteers. Next, the experimental results of preprocessing, QRS wave cluster detection, and the performance of the CNN-based classification model, which achieves a high level of accuracy in a 7-level classification task, are also discussed.

Chapter 5 is a summary of the report, one that highlights the significance of the study, possible contributions, limitations, and potential problems. This chapter highlights the importance of developing lightweight, low-power sleep apnea detection systems for wearable devices and the achievements in designing flexible, self-powered pressure sensors and implementing end-to-end deep learning ECG recognition solutions.

Chapter 6 outlines future work and areas for further research, discussing the importance and need for improvements in a range of issues including sensor output enhancement, stability and integration.

CHAPTER 2: LITERATURE REVIEW

2.1 RESEARCH STATUS IN HARDWARE

With advances in polymer science, thin-film processing and nanotechnology, as well as the development and application of piezoelectric principles, researchers are now able to develop ultra-thin, flexible electronic devices that can be bonded to the skin through van der Waals forces and fit securely into the body without the need for additional adhesives or tapes[7]. Nanogenerators (NGs), which provide energy, are the basis for flexible sensor-driven systems that are self-powered. NGs-based sensing systems are self-powered, flexible, lightweight, and low-cost, and have led to the emergence of piezoelectric nanogenerators (PENGs), friction electromechanical nanogenerators (FENGs), and friction-based nanogenerators (TENGs), which are becoming the key technologies to drive the innovation of wearable and implantable devices in the future[8]. The emergence of these technologies has shown great potential for flexible self-supplying sensors and actuators for future wearable electronics and implantable devices. Combining this technology with today's rapidly evolving Internet of Things (IoT) Big Data and Artificial Intelligence (AI) Machine Learning, NGs-based sensing systems can be the ideal platform for industrial healthcare, smart homes, human services and smart manufacturing[9].

Flexible sensing systems based on NGs in the medical field have already shown some unique places, and the increase that allows them to connect with human health testing is the human skin. The skin is the easiest of the body's organs to collect information from and has the potential to provide a great deal of information about the body's health. The

Researchers intend to deploy flexible sensors embedded in a series of skin-like devices with a polymer support layer to provide diagnostic services for healthcare applications[11]. And now, research has achieved great improvements in device performance, materials exploration, skin integration technology, power supply systems and mechanical design, and has developed a scalable, flexible device capable of delivering clinically relevant data in a variety of applications, including cardiology, dermatology, electrophysiology and sweat diagnostics[12]. This new class of skin-like electronic devices is about to move from the research lab into real-world testing, where they could be more comfortable and not get in the way of everyday life, thus changing the way we monitor our health. It is foreseeable that these devices could one day replace older health monitoring tools in clinics, as they can be applied to the skin to provide accurate and reliable health information[13]. For example, today's research indicates that piezoelectric pulse sensors in combination with approximate entropy (ApEn) analysis can be used to detect people's pulse, which in turn reveals health conditions. Nie et al.[14] utilized a pliable cellular polypropylene (PP) piezoelectric film along with a wooden cylinder base to replicate the procedure of pulse assessment in traditional Chinese medicine (TCM) for capturing pulse features. It was experimentally verified that the ApEn values of the pulse signals obtained under different external forces do not change during the pulse measurement process. Therefore, the sensory system can offer convenient operational protocols for acquiring pulse information with minimal distortion for further analysis. In addition, Lee et al.[15] designed a novel auditory sensor that they hope will be used for sound acquisition in the future to help with health testing. They designed a special sticker-type sensor attached to a person's

neck that would be able to pick up the information generated by the vibration of sound, even if the surroundings are noisy, and do a decent job of collecting information to detect a person's health. The sensor boasts some cutting-edge design and technology. An electret-powered polymer diaphragm with a hole-pattern design is ingeniously utilized, as it transforms into a sensory marvel, seamlessly attaching to the skin. In terms of performance, the voltage bias generated by the devices, which is greater than 400 V compared to the counter electrode, diminishes the need for a large power supply and enables the capacitive sensor to demonstrate increased sensitivity through the addition of an elastomer[16]. The flat frequency response (80-3000 Hz) and excellent linearity (50-80 dz) of the capacitive sensor are also observed. Excellent linearity (50-80 dB SPL) is achieved by the sophisticated capacitive structure with low mechanical damping. The skin-attachable sensor, aided by the hole-patterned electret diaphragms, can detect neck-skin vibration specifically, rather than dynamic air pressure. It has a unique design with holes that focus on neck skin vibrations, allowing it to hear voices in loud environments, and the material Pentium® Pentaplasma®, which is used in the design of the diaphragms[17]. It has a unique design with holes that focus on neck skin vibrations, allowing it to hear voices in loud environments, and the material PDMS nanodroplet is placed on the sensor, increasing its ability to pick up vibrations[18].

To make it more functional and be able to be more widely used in the future, The researchers propose that small wireless signal transmitters could be integrated with their devices in the future to make them more portable[19]. Flexible packaging could

also be used to prevent moisture from affecting the sensing performance of skin-attached sensors based on capacitive changes[20].

However, these technologies still have shortcomings, and their further development in the future will entail: (1) enhancements in engineering and technical aspects; (2) customization of designs tailored to specific applications to ensure dependable and precise diagnostic capabilities; and (3) validation through clinical case studies. [21]. For example, for engineering/technological improvements, progress in wireless power transmission, communication, and seamless/reliable skin integration holds significance. Because for the present, it is recognized that communication stands out as the most energy-intensive operation presently, with duty-cycling in data transmission commonly used to minimize consumption. Current technologies such as low-power Bluetooth can provide reliable connectivity with high resolution in both spatial and temporal domains, however, their current power consumption is excessive (≈5 mW), leading to the need for more energy storage in the system, exceeding the capacity of thin film batteries (<1 mW)[22]. Thus, requiring more efficient energy transfer and storage solutions. The optimal method for achieving high-performance wearable electronics is through the utilization of the hard-soft integration strategy, which provides reliable power and communication solutions[23]. When it comes to the problems encountered in this area, the main challenges are the development of thin-film interconnects, efficient packaging, and the use of low-modulus materials to maintain the mechanical integrity of the device[24].

The utilization of adaptable electrets can also serve a crucial function in applications related to human-machine interaction, such as augmented reality (AR) and virtual

reality (VR), as flexible wearable devices need to be able to detect and generate mechanical stimuli that enable people to feel a deeper sense of immersion in the AR and VR experience[25]. In that respect, in previously studied devices, the performance could not meet the demand resulting in small stimuli generated and insufficient feedback data received, which is due to the difficulty of a simple single structure to have a high charge density, and a larger equivalent piezoelectric coefficient is the key to improve the performance of the actuator and sensors, which includes increasing the sensitivity of the sensors and decreasing the actuator drive voltage[26]. Research done by Zhong et al.[27] has been able to utilise sandwich-structured piezoelectret to enable excellent performance, providing a good basis for sensor and actuator functionality. As expected, experiments and simulations have demonstrated that by improving the shape of the device and using better materials, such as making it thinner and increasing the space, the charge of the FEP film can be increased, effectively improving the piezoelectric effect, and working performance of the device. In the future, better structural designs such as honeycomb structures or materials with larger maximum charge density values can be used to further improve the performance[28].

Nowadays, the sensing and actuation systems based on NGs face many challenges: 1) To begin with, the sensor is integrated into the output improvement and retention processes, ensuring precise assessment of the output, stability, downsizing, and incorporation, among other factors. In terms of output power, the output power density of NGs is now tens of milliwatts per square meter, and greater output power is needed[29]. Researchers initially suggested that enhancing the output power could be achieved through techniques such as doping other materials, modifying interfaces,

treating surfaces, and adjusting the equivalent density[30], but it is not concise enough to be effective. Evaluation of the output with accuracy, however, is attributed to the interfacial slippage among high triple-charge-density polymers in the PENG device, leading to triboelectric outputs as discussed by Harmon et al.[31] suggest a possible solution: by utilizing discrete semiconductor components such as silicon-controlled rectifiers and Zener diodes, Fan et al. developed NGs without the use of integrated electronics.[32] show that the sensors can be used in ambient environments after 100,000 loading-unloading cycles. According to Fan et al.[32], the sensors demonstrated remarkable stability in normal conditions following 100,000 cycles of loading and unloading. However, going forward, it will be essential for the sensors to exhibit this trait in challenging environments characterized by high levels of humidity and temperature. It is worth noting that existing technologies already have PENGs that can maintain effective performance in harsh environments with extremely high temperatures[9]. 2) Friendliness to the environment and compatibility between the device and the human body, as well as comfort and aesthetics, are also areas of concern for future development. Among the different comforts, breathability is getting more and more focus because of its capacity to control the balance between water and heat. One possible method is to create some 3D micro/nano layer pores on the film's surface or to incorporate specific gaps between the multiple layers. For the environment, one solution has been reported to be the use of all-nanofibers as a material. Such devices have shown good biodegradability. It is important to mention that good biodegradability can result in low outputs. Therefore, the search for new materials or the establishment of appropriate recycling mechanisms may not be a bad solution[28].

2.2 Research Status in Signal Processing

In ECG signals, each heartbeat of the human body is reflected as a heartbeat, the main components of a single heartbeat include P-wave, Q-wave, R-peak, S-wave, T-wave, of which Q-wave, R-peak and S-wave are collectively called the QRS wave complex[33]. It has been shown that the modulation of respiratory signals in ECG signals includes baseline drift, amplitude modulation and frequency modulation[34]. As one of the most significant features of ECG signals, the above three modulations of respiration affect the amplitude, position, and morphology of the QRS wave clusters. In particular, the amplitude characteristics of the R-peak are highly correlated with the respiratory signal[35] and have been widely used in studies related to respiratory signals[36]. Therefore, for sleep apnea detection from ECG signals, it is first necessary to accurately detect the QRS wave clusters (or R peaks) from ECG signals.

Due to the wide variety of physiological characteristics of different users, the acquired ECG waveforms are not identical[37]. Even for the same user, the waveforms may change depending on the location of the ECG patch. In practice, the accurate detection of QRS waveforms is not only affected by the morphology of QRS waveform clusters, P-waves, and T-waves but is also susceptible to various noise interference[38]. For example, muscle noise due to human muscle activity, motion artefacts due to electrode movement, and baseline drift due to multiple reasons. These factors may cause the algorithm to mistakenly detect other waves (e.g., P- and T-waves) as R-peaks (False Positive, FP), or determine R-peaks as other waves resulting in missed detection (False Negative, FN).

Most of the existing QRS detection algorithms can be divided into the following steps: preprocessing, feature enhancement and judgement[39]. Existing research has focused on improving the algorithms by optimizing these three steps.

The main purpose of preprocessing is to minimize the noise component in the ECG signal. The main effective components of the ECG signal are in the spectral range of 0.5 to 50 Hz[40], and the ideal frequency band to maximize the energy of the QRS wave population is about 5 to 15 Hz[41].

The Pan-Tompkins algorithm is one of the most classical algorithms for QRS detection algorithms. The algorithm consists of a bandpass filter by cascading a low-pass filter with a cutoff frequency of about 11 Hz and a high-pass filter with a cutoff frequency of about 5 Hz[42]. Nayak et al. simulated the fractional-order differentiator by using an infinite Impulse Response (IIR) filter with a step of 0.1. Nayak et al. used the Infinite Impulse Response (IIR) filter to simulate a fractional order differentiator with 0.1 steps and tried the effect of 0.1 to 1.5 order differentiators on the detection results in turn and found that 0.5 order achieves the highest accuracy[42]. Wavelet transform is widely used in QRS detection algorithms. As an alternative to the Fourier transform and the short-time Fourier transform, it is capable of extracting information on both time and frequency scales[44]. A variety of wavelets have been available in existing research results, such as the Mexican hat wavelet[44], Mortlet wavelet[45], Daubechies wavelet[46], etc. Although the wavelet transform can extract rich information, not only filtering out the noise but also directly skipping the step of feature enhancement for direct judgement[46], the arithmetic complexity is too high.

In the original ECG signal, even though the R peak is in general the wave with the highest amplitude, the direct detection of the amplitude will reduce the accuracy and robustness of the algorithm due to the influence of baseline drift and T-waves of various morphologies. Therefore, it is necessary to further enhance the R-peak or QRS wave group features (e.g., slope) through various transformations, i.e., feature enhancement. The Pan-Tompkins algorithm first highlights the slope information of the signal by making a difference between neighbouring samples, and then squares it to further highlight locations with high amplitude[41]. However, directly solving for slope makes the algorithm susceptible to noise such as burrs, and therefore sliding average filtering is required for smoothing Tekeste et al. used Curve Length Transform (CLT) to enhance the QRS wave group features[40].

The final step is the threshold-based judgment. Many studies adaptively determine the threshold based on the amplitude of the R-peaks that have been detected in the previous time[41]. Kaur et al. proposed a method of backward search. If no QRS wave clusters are detected near the time point of the mean RR interval, a lower threshold (0.25 times the original threshold) is used to start the search again from the previous QRS wave cluster to reduce missed detections (FN)[40]. It is also necessary to ensure that the newly detected QRS wave clusters are more than 200 ms away from the previous QRS wave clusters to avoid misdetection of T-waves as QRS wave clusters and increase FP. In the Pan-Tompkins algorithm[41], if no QRS wave clusters are detected in a specific period, the largest peaks occurring in that time will be determined as QRS wave clusters. In addition, after a QRS wave group is detected, peaks larger than a threshold value for a certain period are blocked to avoid FP due to T-waves, i.e., the inopportune period

mechanism. In the work of Manikandan et al., the Hilbert transform is used to detect QRS wave groups by detecting the over-zero points[46]. However, both the normalization and Hilbert transform in this algorithm are non-causal systems and need to be processed uniformly after obtaining all the ECG signals, which is not real-time, although it can achieve good accuracy and robustness. When applied to wearable health monitoring devices, the storage of a large amount of ECG data not only requires a large amount of storage space but also generates a lot of area and power consumption overheads.

After the QRS wave clusters have been detected, appropriate information needs to be extracted from them to complete further classification to determine whether a sleep apnea event has occurred during the period. A 1995 study showed that apnea during sleep leads to a decrease in SpO_2, which affects the autonomic nervous system and results in Heart Rate Variability (HRV)[47]. In addition to HRV, ECG-derived Respiration (EDR) is a commonly used feature to detect sleep apnea, mainly in the amplitude of the R-peak. As for the classification methods, the existing sleep apnea algorithms can be mainly classified into two categories: traditional machine learning methods and emerging artificial intelligence methods.

Yeo et al. performed Symlet wavelet decomposition of ECG and respiratory signals, and then extracted 135 features from them to be used in several traditional machine learning algorithms for classification, including Linear Discriminant Analysis (LDA), Quadratic Discriminant Analysis (QDA), Stochastic Mori Analysis (SMA), and Randomized Mori Analysis (RMA), which were used to classify the ECG and respiratory signals. The experimental results show that SVM can achieve the best

classification results, with an accuracy of 80-85% on multiple datasets[48]. Surrel et al. extracted the RR interval and R-S peak amplitude of ECG signals, and then used them for the classification of the ECG signals. interval and R-S peak amplitude of ECG signals calculated the spectra of the two and used SVM to classify the signals with an accuracy of 85.7%[49].

Sheta et al. obtained an accuracy of 85.7% by finding 9 features such as average heart rate, standard deviation of RR interval sequence, and so on. 13 machine learning algorithms such as Decision Tree (DT), K-nearest Neighbor (KNN), and 4 deep learning models were combined to make a judgement with an accuracy of 86.5%[50].

Recently, artificial intelligence (AI) has seen rapid development and wide application in fields such as computer vision (CV), natural language processing (NLP), and medical health monitoring, because of its notably powerful capabilities for automatic learning and extracting deep latent information[51].

Wang et al. classified electrocardiogram (ECG) signals based on extracted RR intervals and R peak amplitudes using a multi-scale convolutional neural network (CNN) with kernels of varying sizes, achieving an accuracy of 85.2% by capturing both fine-grained and global features[52]. Rajabrundha et al. experimented with CNNs, gated recurrent units (GRUs), and long short-term memory (LSTM) networks, finding that LSTMs performed best with an accuracy of 85.6%[53]. Sharan et al. employed raw single-lead ECG signals as input to a residual network containing six residual blocks, each with three convolutional layers, resulting in a highly accurate classification rate of 93.05% [54]. Furthermore, Nguyen et al. detected S waves following R peak detection and classified features including R and S amplitudes, RR intervals, and SS intervals (the

interval between adjacent S waves) after median filtering, obtaining 91.13% accuracy using a 50-layer residual network called SE-ResNext-50[55].

2.3 Conclusion

In general, some of the existing QRS detection algorithms are too complex and difficult to implement in hardware, which makes them difficult to apply to wearable devices; some of them need to acquire the whole ECG signal for processing, which cannot meet the real-time requirements; some of them can solve the above problems, but the accuracy is not very satisfactory. In terms of sleep apnea detection algorithms, traditional machine learning algorithms rely on the extraction of many artificial features. This type of method requires manual selection and testing of features, which is highly subjective and limited by the performance of the classifier, often with limited accuracy. Emerging AI algorithms can automatically learn deep features, which ensures objectivity and robustness, and at the same time can achieve a high accuracy rate.

CHAPTER 3: EXPERIMENTAL DESIGN

3.1 Design Strategy

One of the main challenges is to fabricate a pressure sensor that can be triggered by tiny pulse vibrations and demonstrate superior mechanical properties and stability. Most existing electrostatic sensors have been made of a wide range of piezoelectric materials such as polyvinylidene fluoride (PVDF), lead zirconate (PZT), poly (dimethyl siloxane) (PDMS) or its copolymers, and zinc oxide (ZnO) to sense various range of mechanical signals, especially pressure and strain. However, PDMS and PVDF have relatively low electrostatic charge densities, leading to low surface potentials. Eventually, these sensors cannot feel the tiny pressure difference and generate noise in the low-pressure range required for pulse detection.

One of the foremost challenges in pressure sensing research is developing a device capable of precisely detecting minute pulse vibration inputs while also exhibiting robust mechanical and structural integrity over time. Previously explored electrostatic sensors have incorporated a wide spectrum of piezoelectric materials, such as polyvinylidene fluoride (PVDF), lead zirconate titanate (PZT), poly (dimethyl siloxane) (PDMS) and its copolymers, and zinc oxide (ZnO), to perceive diverse mechanical stimuli like stress and strain. However, both PVDF and PDMS possess inherently low surface charge densities that translate to weak electrostatic polarization. As a result, sensors consisting only of these constituents may struggle to differentiate tiny pressure differentials and are predisposed to noise interference within the narrow low-pressure ranges required to identify pulse waveforms.

The simplest strategy to adhere flexible devices on skins is to choose materials (e.g., PDMS, Ecoflex, Solaris) that have an elastic modulus close to that of the skin. In this way, these layers would enable a pleasing human-sensor interaction.

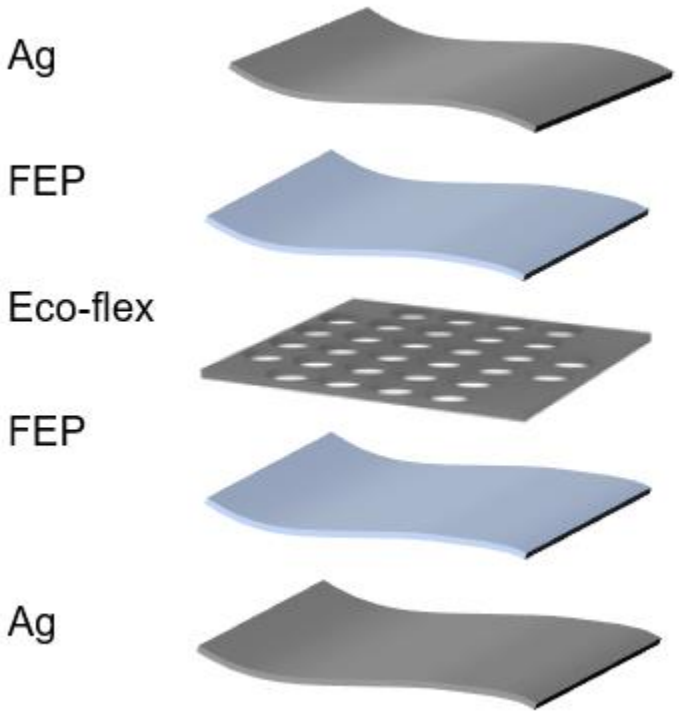

Figure 3.1 Exploded-view schematic illustration of the sensor.

Hereby, we summarize all demands and design a device that features a flexible, sandwich-structured utilizing piezoelectret materials in this study. The design of this self-powered sensor incorporates an ultra-thin piezoelectret device featuring an optimized parallel capacitor configuration. The materials and structure of the sensor are shown in Figure 3.1. Specifically, two 4×4 cm^2 Ag electrodes are plated on both sides of the sensor on the surface of the FEP films. Silver is excellent in electrical conductivity can be used as an electrode surface layer and is a biocompatible substance

that can be used as a surface for long-term contact with the human body. Fluorinated ethylene propylene (FEP) has shown potential as an electret material for piezoelectric energy harvesting devices due to its ability to maintain electrostatic polarization over long durations. When using silver-coated FEP films (Ag/FEP), we characterized the decay behavior of the implanted surface charge by quantifying the sample's temporal surface potential via non-contact charge probe measurements. The detailed preparation processes of the SFS (Self-powered flexible sensor) are demonstrated in Figure S3.

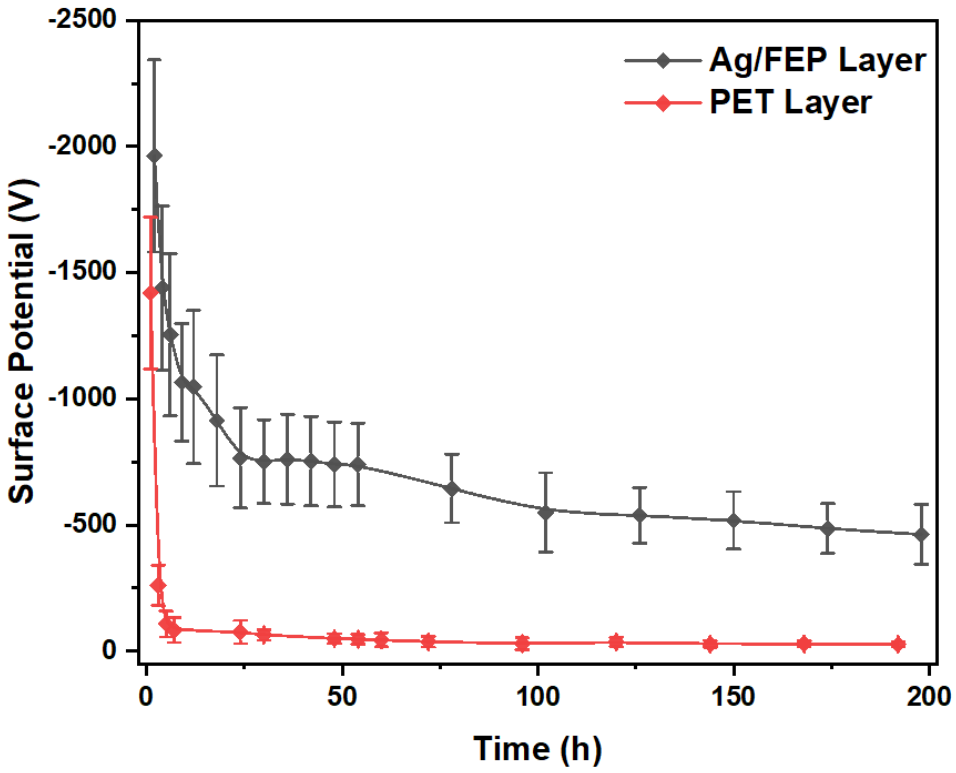

Figure 3.2 Comparison of surface potential decay for FEP and PET

As illustrated in Figure 3.2, the negative surface charge on Ag/FEP composites exhibited only gradual decay when monitored for extended time intervals post-charging, rather than abrupt reductions in stored energy. The schematic diagram of the measuring

method is demonstrated in Figure S2. During the 200 hours of continuous testing, the initial surface potential values of the Ag/FEP layer was about 2000 V. It dropped swiftly to -767V from -1962V in the first 24 hours. Then there was a consistent slow decline in the rest of the 175 hours. While the surface potential of PET plummeted to -261V within 2 hours, then it maintained the same level. The capability of the Ag/FEP layer for retaining charges was in stark contrast with that of the PET layer. This favourable retention characteristic could enable the design of self-powered systems capable of sustainable operation through intermittent mechanical vibrations or other periodic stimuli.

A corona charging process was used for generating megascopic electrical dipoles inside the air cavities in the Eco-flex layer. As shown in Figure S4, in the negative corona charging process, the ambient atmosphere was broken down due to the high external electric field. The electret film trapped negative charges on its upper side. Especially, a thinner spacer layer and a higher cavity-to-spacer area ratio could both improve the piezoelectricity. However, if the spacer layer is too thin or the cavity to the spacer area ratio is too high, the top and bottom FEP layers may contact each other under a mechanical deformation.

Previous testing revealed that a piezoelectret film with 150 μm thickness and 39.8% cavity-to-spacer area proportion exhibited stable equivalent d_{33} coefficient quantification of 4050 pC/N, which is much higher than those of former published piezoelectric and piezoelectret materials, such as cellular PET[56]. The difference in peak output voltage between FEP and PET is shown in Figure S1.

Double-sided tape was used to securely bond the four corners of the fluorinated ethylene propylene (FEP) films, thereby forming an inner air cavity within the ultra-thin sensor structure. Both the amplitude of electrostatic charges deposited on the FEP surface and variations in air gap thickness induced by external mechanical stimulation were significant factors influencing sensing performance. As illustrated in Figure 3.3, the total sensor thickness measured approximately 300 μm. Owing to this exceedingly thin thickness, the device exhibited a high degree of intrinsic flexibility and negligible mass (at 1.0 grams). The extreme malleability and lightweight attributes endowed the sensor with the capacity to discern subtle mechanical pressure transients such as pulses. By minimizing the sample mass while capitalizing on localized charge-gap change conversion, a design conducive to discriminating minute input stimuli was realized.

Figure 3.3 Optical photo showing the thickness of the sensor.

3.2 WORKING MECHANISM

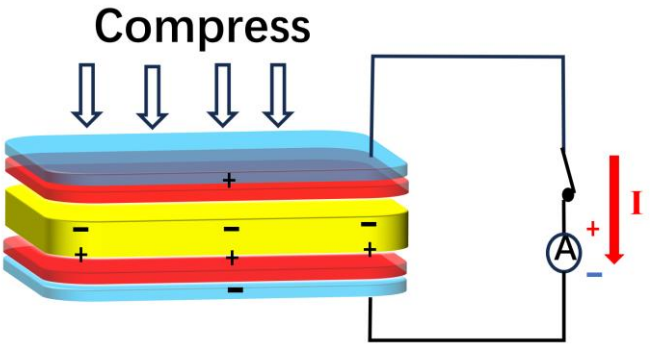

Figure 3.4 The working mechanism of generating electrical current due to the vibration.

The external surfaces of the flexible piezoelectret sensor structure were coated with 50nm thick silver films to serve as electrodes. As a pressure sensor, compressing and releasing it will change the distance of the air gap and the moments of the megascopic electric dipoles, as indicated in Figure 3.4, leading to the transformation from mechanical deformations to electrical signals. According to the model depicted, applied mechanical stresses of $\pm\sigma_0$ facilitated electrostatic induction, generating induced surface charges ($\pm\sigma_E$) on both silver electrode interfaces. When a pulse was applied to the sensor, the change in the dipole moment affected $\pm\sigma_E$. The charge fluctuations motivated free electron flux within the electrodes to produce direct current outputs, thus achieving transduction of mechanical stimuli to electrical signals. The equivalent d_{33} of a 4×4 cm^2 was estimated at 4000 pC $N^{-1}cm^{-2}$[56], suggesting efficient mechanical-electrical signal transformation ability.

At any moment in the entire working process of a sensor, $\pm\sigma_E$ is determined by the following equation:

$$\sigma_E = \frac{\epsilon(\pm\sigma_0)}{(\frac{2d_0}{\Delta d} + \epsilon)} \tag{3.1}$$

where Δd is the air gap thickness in the sensor, and d_0 and ε are the thickness and relative dielectric constant of the FEP layer.

A higher value of σ_E/σ_0 for an air gap variation value indicated that more free electrons were transferred to the external circuit, resulting in a higher output voltage.

3.3 Electrical System

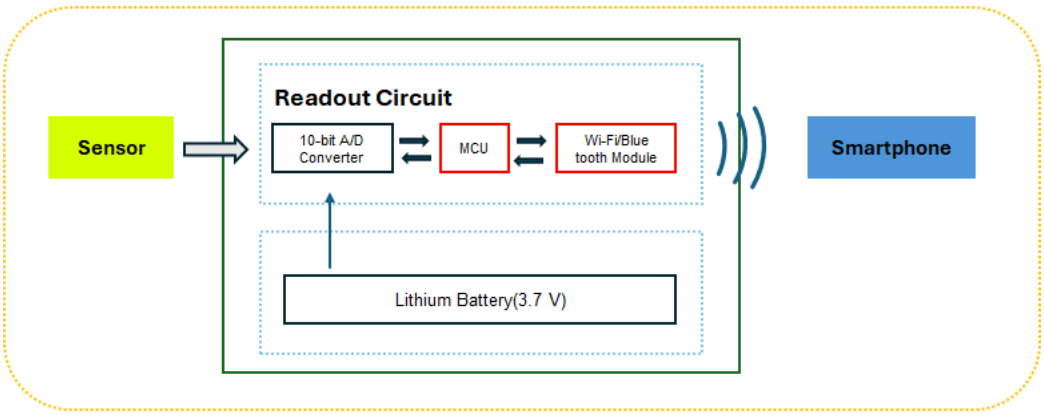

Figure 3.5 Block diagram of the system.

The sleep heartbeat monitoring was developed by uniting an ultrathin self-powered pressure sensor as a pulse detection sensor, a circuit based on an Arduino board (ESP32D-V4 CH9102X), and a power supply unit (3.7V, 16340 lithium battery), as illustrated in Figure 3.5.

The readout circuit was designed with an optimal impedance match for our sensor, primarily consisting of a 10-bit analog-to-digital (A/D) converter, a low-power microcontroller unit (MCU) based on the 32-bit Arm Cortex-M0 architecture

(SAMD21), and a WiFi module known as NINA W102 ESP32. Additionally, an advanced version, ESP32D-V4 CH9102X, was incorporated into the circuit for enhanced functionality and performance. It contained two channels (DAC1 and DAC2) that could transform digital values into corresponding analog voltage outputs. Managed by five dedicated converter controllers, it measures analog signals from 18 pins, as well as internal signals such as vdd33.

The initial step of the ADC conversion involves configuring the control registers to define various operational parameters. It includes the selection of conversion mode (single/continuous), resolution (8/12 bits), input attenuation (0-11x gain), and clock prescaling. Additional options such as enabling onboard temperature sensing and designation of sampling channels are specified.

Initiation of the conversion process involves invoking commands such as adc1_get_raw and adc2_get_raw to read the 12-bit raw codewords from Channels 1 and 2. These digital representations require post-processing to obtain actual voltage values. Such processing entails applying the calibration coefficients accessed earlier to normalize codewords and compensate for instrumentation non-idealities.

3.4 Deep Learning Model

The rise of deep learning has provided a solution for ECG recognition, i.e., instead of manual filtering and feature extraction, the ECG data can be sliced and diced and fed directly into a model for classification. The classical convolutional neural network plays the role of feature extraction, where each convolutional kernel is equivalent to a filter, filtering out the signal containing information from the original signal.

3.4.1 Data Set Acquisition

At present, there are four most important and authoritative ECG databases in the international arena: MIT-BIH ECG Database: jointly established by the Massachusetts Institute of Technology (MIT) and Beth Israel Hospital (BIH) in the United States[57]; AHA Arrhythmia ECG Database: established by the American Heart Association (AHA); CSE ECG Database: established by the European Union (EU); and EU ST-T ECG Database. In addition, the Sudden Cardiac DeathHolter Database and other ECG databases are widely recognized internationally. As indicated in Figure 3.6, PhysioNet provides a simple and convenient web-based version of the conversion tool PhysioBank ATM (*https://archive.physionet.org/cgi-bin/atm/ATM*)[58]

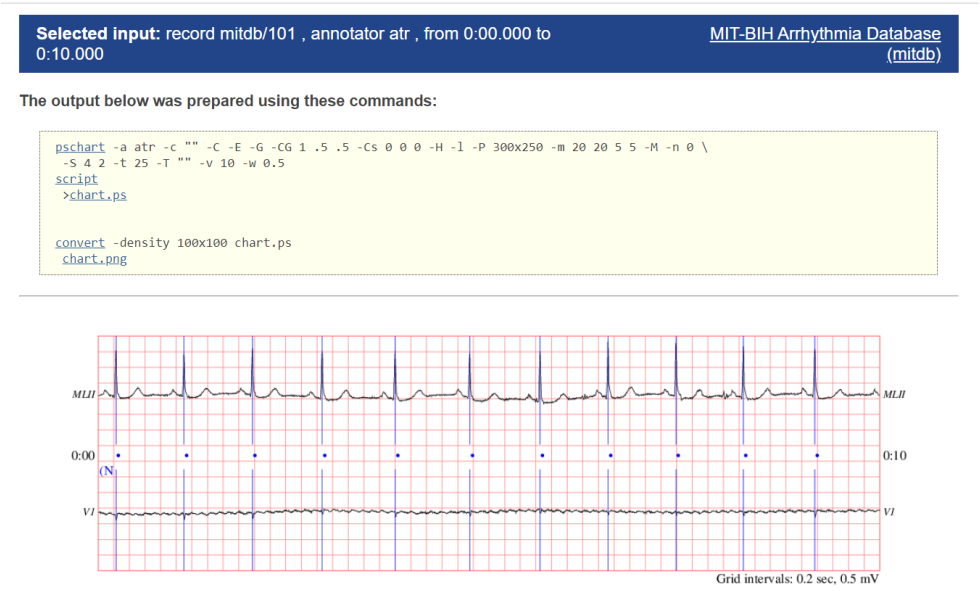

Figure 3.6 Screenshot of using PhysioBank ATM.

To evaluate the effectiveness of the ECG preprocessing algorithm, the sleep apnea detection algorithm and the convolutional neural network structure proposed in this paper in sleep scenarios, the Apnea-ECG dataset is used for relevant experiments and validation[59]. This dataset is derived from the CinC Challenge 2000 competition, which

is widely used in the field of sleep apnea detection, and contains 70 ECG data collected from patients and normal users during sleep periods, ranging from a little less than 7 hours to 10 hours, with a sampling rate of 100 Hz, of which 35 are officially classified as the training set (classified as groups a, b, and c), and 35 are classified as the test set (recorded as a group a, b, and c). Each minute of all ECG data was labelled by an expert as to whether a sleep apnea event had occurred in the current minute, with "A" indicating that it had occurred and "N" indicating that it had not.

3.4.2 Data Pre-Processing

The ECG signals in the database may contain noise during the acquisition process due to various factors, which reduces the quality of the ECG signals and to a certain extent affects the medical or computer recognition of apnea. An interference signal generated by a change in electrode position due to human respiratory motion, generally below 1 Hz, causes the ECG signal to fluctuate up and down.

Hence firstly, a high filter is configured by the following code:

```
b, a = signal.butter(8, 0.007, 'highpass')
```

Next, the signal is filtered using the signal.filtfilt function:

```
ecg_1 = signal.filtfilt(b, a, bw_denoised)
```

Then, a lowpass filter is configured by the following code:

```
b, a = signal.butter(8, 0.1, 'lowpass')
```

Finally, the filtering operation is performed on the signal by using the filtfilt function again:

```
denoised_ecg = signal.filtfilt(b, a, ecg_1)
```

3.4.3 R-WAVE DETECTION

R-wave is the most obvious feature of the ECG signal, and it is also the basis for extracting the features of the HRV signal. Only when the R-wave is detected accurately, the heart rate can be calculated, and then the features can be extracted. Therefore, the accurate detection of R-wave has an important impact on the detection of SAS. For the detection of R-wave, wavelet decomposition[60], band-pass filtering[61], and difference methods[62] are commonly used. The band-pass filtering method applies a band-pass filter on the ECG signal that can extract the specific frequency of the R-wave, making the characteristics of the R-wave more obvious and easier to find the peak point, but it is prone to leakage detection. The principle of the differential method is simple, clear, and easy to operate, but it has poor anti-interference ability. Wavelet splitting and solving method is very favoured by most research scholars because it solves the problem of window transformable, but it is complicated to operate.

3.4.4 WAVEFORM FEATURE EXTRACTION OF ECG SIGNAL BASED ON CNN

The WFDB (Waveform Database) toolset is a highly portable software package written in C that allows for reading, writing, and processing of WFDB signal and annotation databases across popular operating systems. The WFDB library facilitates signal processing and automated analysis, while the WAVE software supports visualization, annotation, and interactive waveform examination. To access header information, the rdheader() function parses .hea files and populates an object with metadata including the number of records, signal channels, and record duration. ECG and other waveform data are obtained via rdrecord(), returning a record object. Important parameters

include record name/path, start/end sample indices, and channel selection. Signal sampling properties like frequency, length, and stored digital/analog arrays can then be directly accessed from record attributes. Finally, annotations are loaded from .atr files using rdann(), providing diagnostic label positions and codes.

We reproduced one of the more highly cited papers in the field, *A deep convolutional neural network model to classify heartbeats*[63], which used only a simple convolutional neural network to achieve 94% accuracy. The convolutional neural network structure used in this chapter consists of four convolutional layers, three pooling layers, and one fully connected layer. The description of each layer is as follows:

Input layer: The input of each minute segment of the Apnea-ECG database intercepted by annotation and then median filtered to remove baseline drift, with an equal number of SAS and normal samples.

Convolutional Layer: The convolutional layer has multiple filters in it to extract local features at the same location. It does not need to consider the global features but only need to extract to a certain region of the features, and then through the constant sliding window extract all the feature information of the ECG signal, and at the same time, it can achieve the weights sharing on the same layer, which allows the network to become deeper under the premise of guaranteeing the efficiency of the computer computation to get more and more detailed feature information[63]. The convolution layer takes the feature vectors of the overall input data and the same set of weight parameters and adds

the bias values after the convolution operation to get the output vectors with feature information.

$$V = conv(W, X) + b \tag{3.2}$$

$$Y = \emptyset(V) \tag{3.3}$$

where *conv* is the convolution operator function, *W* is the convolution kernel matrix, *X* is the input data matrix, *b* is the bias and *V* is the output of the convolution operation. Equation (3.3) feeds *V* as input to the activation layer and Φ is the activation function.

Activation Layer: this layer performs thresholding operations based on a nonlinear decision mapping function, which increases the ability of the whole model to express features. In this chapter, the ReLU function with strong training performance is used as the activation function. When the feature value extracted from the convolutional layer is less than or equal to zero, the output is zero; when the feature value is greater than zero, the output itself. Setting the threshold, not only improves the computational efficiency of the computer but also avoids the problem of high computational cost.

Pooling layer: the convolutional layer generates many parameters after extracting the features. Therefore, adding a pooling layer after the convolutional layer reduces the number of parameters and reduces the computational pressure. There are two types of pooling operations: average pooling and maximum pooling. Average pooling is to calculate the average value of each region to form a new feature vector matrix. On the other hand, maximum pooling can obtain more distinctive features by performing

sliding dimensionality reduction on all feature vector matrices and selecting the maximum value in each sliding region to form a new feature vector. Therefore, the maximum pooling operation is chosen in this chapter, which not only can effectively reduce the feature dimension and keep the most expressive features but also can reduce the risk of overfitting.

Fully Connected Layer: the fully connected layer is generally at the end of the entire network and serves to integrate features. It can map the abstract features extracted from the hidden layer neurons to the labelled space of the data and then express them visibly[63].

The number of layers in each layer of a convolutional neural network and the parameter values set not only affect the number and depth of features extracted but also have a significant impact on the speed and quality of classification. The denoised ECG signals were input into several different layers of convolutional neural networks and their parameter values were adjusted and optimised. After repeated adjustments and modifications, the structure of convolutional neural network consisting of three convolutional layers, three pooling layers and one fully connected layer was finally determined to be suitable for the research of this topic. The specific parameter settings for each layer are shown in Table 3.1.

Layers Count	**Layer Type**	**Convolutional**	**Number of**	**Stride**

		Kernel	Kernels	
Layer 1	Input Layer	-	-	-
Layer 2	Convolutional Layer	21×1	4	-
Layer 3	Pooling Layer	3×1	4	2
Layer 4	Convolutional Layer	23×1	16	-
Layer 5	Pooling Layer	3×1	4	2
Layer 6	Convolutional Layer	25×1	32	-
Layer 7	Pooling Layer	3×1	4	2
Layer 8	Convolutional Layer	27×1	64	-
Layer 9	Dense Layer	-	-	-

Table 3.1 Convolutional neural network structure specific parameters

3.5 CONCLUSION

In this chapter, we discuss the experimental design process for developing a self-powered flexible pressure sensor and a deep learning-based approach for ECG recognition. Firstly, we focus on the use of piezoelectric materials (e.g. FEP and silver electrodes) to create sandwich-structured sensors with optimized shunt capacitor configurations and explain the mechanism of operation of the sensors, with an emphasis on the process of converting mechanical deformations into electrical signals. The integration of the electrical system, including the self-powered pressure sensor, the Arduino board and the Li-ion battery power supply, and the readout circuitry designed with optimal impedance matching are then described. In addition, we discuss deep learning models for ECG recognition, including data acquisition from the MIT-BIH

arrhythmia database, preprocessing techniques such as filtering, R-wave detection methods, and feature extraction using CNN architectures to lay the foundation for our experimental work.

CHAPTER 4: RESULT AND DISCUSSION

4.1 Sensor Performance Evaluation

4.1.1 Durability and Reliability Testing

Sample sensors were placed in a constant temperature drying oven at 85°C relative humidity for 24 hours, then placed for 24 hours in an environment with 82% humidity to accelerate the ageing process. Then, sensors underwent a durability test with a frequency of 1Hz for over 10000 cycles. The test platform was built for collecting the output voltage of the SFS, as illustrated in Figure S5. The middle 50 minutes of data collection is shown in Figure 4.1. It is seeable that the output current remains stable though a tiny variation within 2% in the time waveforms, demonstrating good stability. The flexible piezoelectric sensor has excellent durability and long-term reliability and can maintain stable performance under harsh environments and repeated workloads, which provides a strong guarantee for its long-term reliable operation in practical applications.

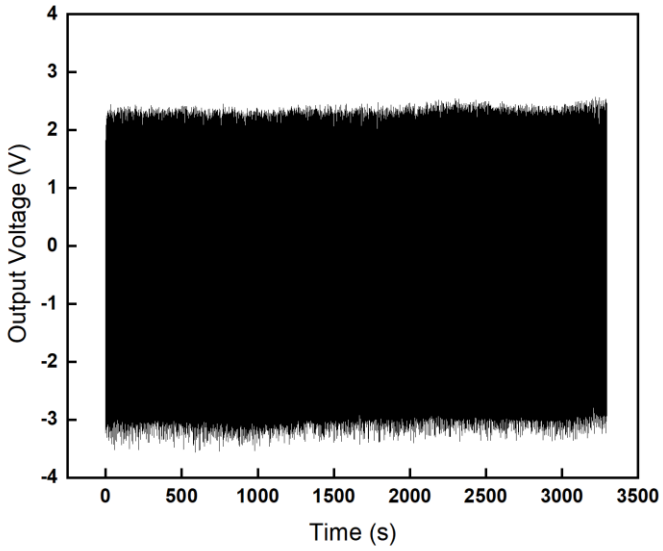

Figure 4.1 Output voltage under an applied periodic pressure.

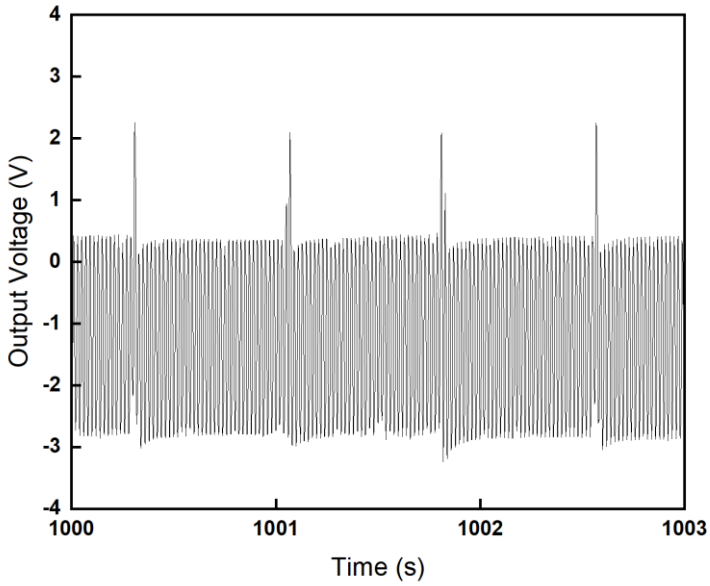

Figure 4.2 Expanded output voltage during the long-term stability test.

4.1.2 Pressure Sensitivity Testing

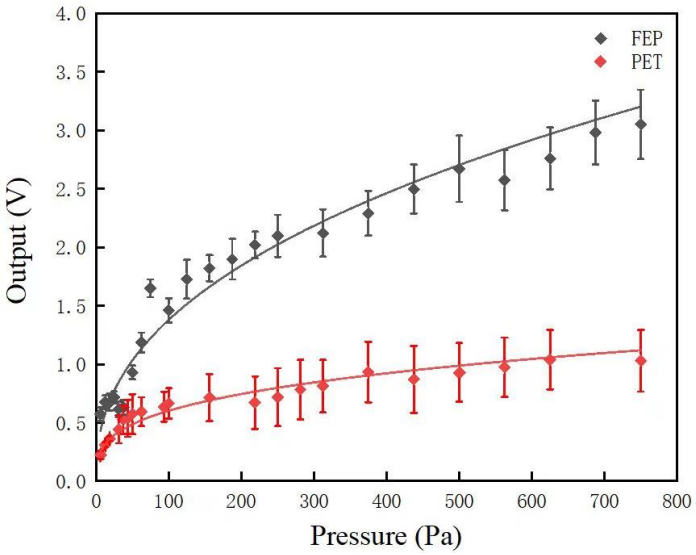

Figure 4.3 Output voltage under pressure within 800 Pa.

During the test, we applied a pressure range from 0 to 750 Pa to the sensor and measured the output values of the sensor at different pressures. Figure 4.3 shows the pressure-output curves of the sensors using FEP and PET respectively.

The voltage slope for the pressure witnessed a downward trend, with an initial value of nearly 8.33V/kPa to 2.51V/kPa after 500 Pa. The sensitivity of the sensor in the range of within 1kPa ensures that it can detect tiny pulse signals.

4.1.3 TESTING WITH STEP INPUTS

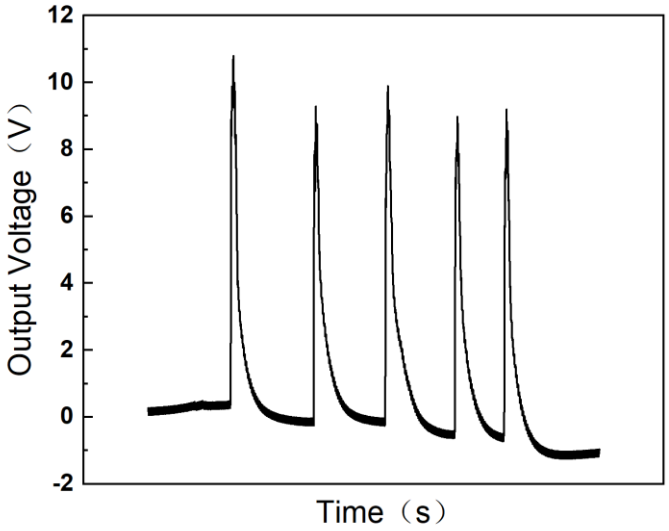

Figure 4.4 Output voltage under sudden input

We tested the dynamic characteristics of the sensor by repeatedly applying large pressures. After calculation, we get the mean value: Response time: 0.0419s; Time constant: 0.0244s; Rise time: 0.0227s.

4.1.4 SELF-POWERED SLEEP PULSE MONITOR TESTING

Figure 4.5 Photo showing the sleep pulse-monitoring process.

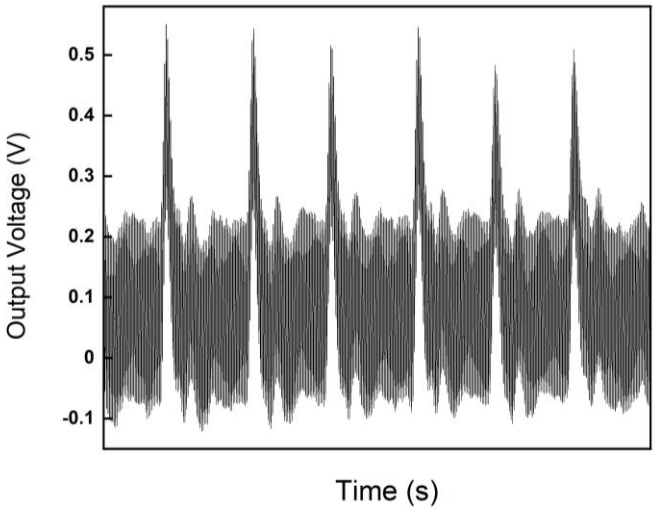

Figure 4.6(a) Photo showing the normal pulse signal in a sleep test.

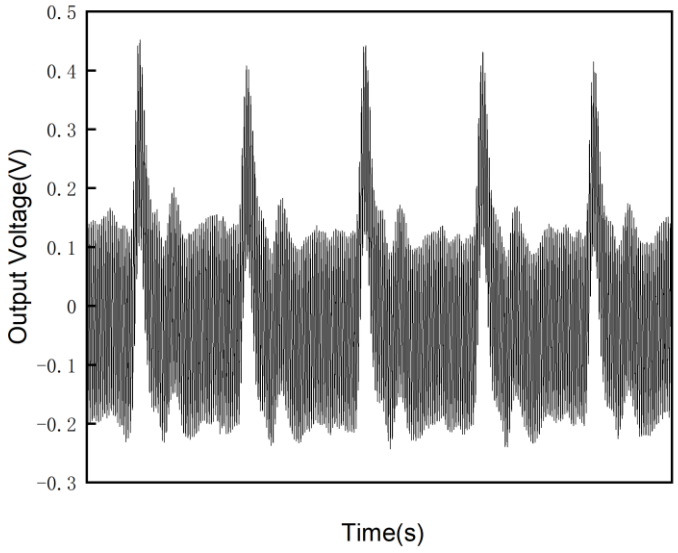

Figure 4.6(b) Photo showing the simulated apnea pulse signal in a sleep test.

We set up a sleep testing platform to validate the application scenarios we envisioned as shown in Figure S6. A specific self-powered pulse-monitoring process for volunteer 1 (male, 21-year-old) is shown in Figure 4.4, where the sensor was fastened on the cloth. The average peak output amplitude for a normal pulse was larger than 0.5 V. We let the volunteer hold his breath for one minute to simulate apnea. Normally, for the same volunteer, an abnormal breath rate has specific characteristics that can be easily identified.

4.2 Algorithm Validation and Performance Evaluation

4.2.1 Experimental Results of Preprocessing

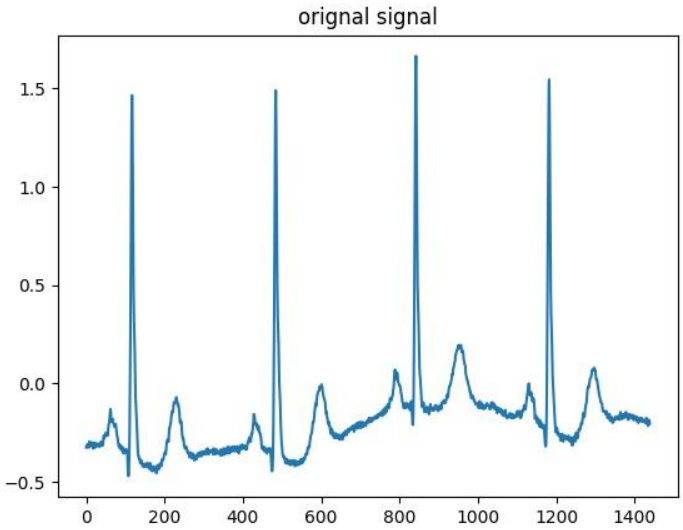

Figure 4.7(a) Fragments of the original ECG signal.

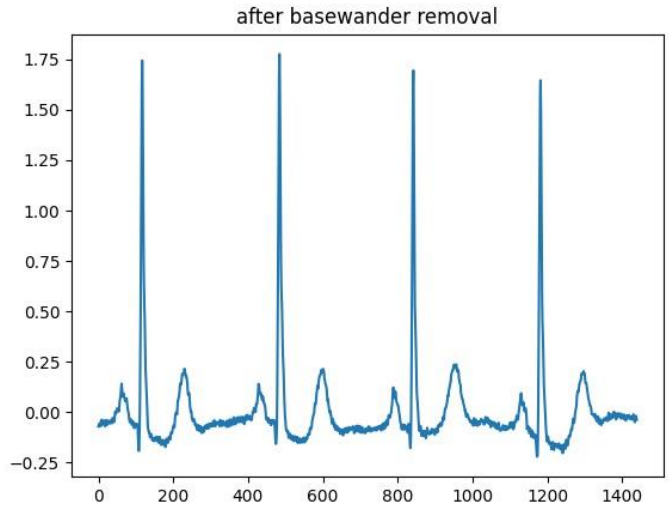

Figure 4.7(b) Suppression effect of the filter on baseline drift in ECG data

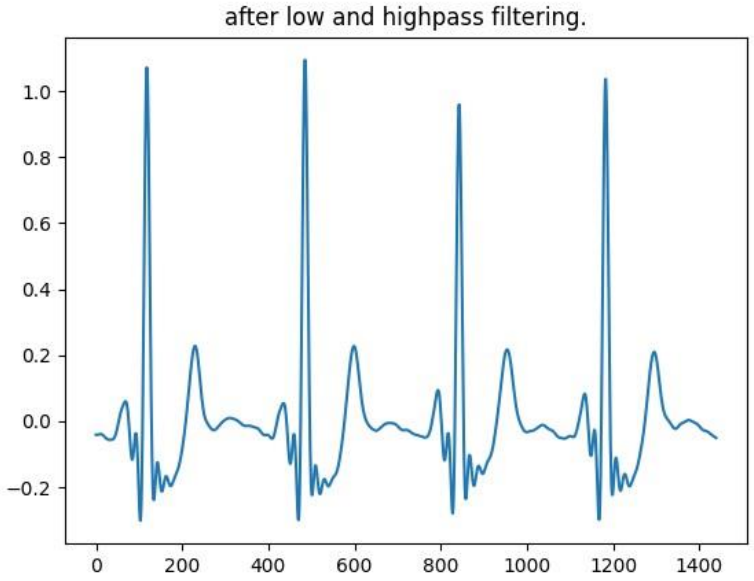

Figure 4.7(c) Fragment of filtered ECG signal

Some of the ECG recordings in the MIT-BIH Arrhythmia dataset are affected by some noise due to various external factors, and the effect of the filter can be demonstrated to a certain extent by applying the designed filter to this part of the signal and comparing it with the pre-filtered signal.

Firstly, as shown in Figure 4.8, this segment of the signal is derived from ECG data a05 in the publicly available Apnea-ECG dataset[59]. There is a fluctuation of -0.3 to 0.3 mV in the baseline of the original ECG data. After filtering, the baseline of the signal is basically around 0 mV. This shows that the designed filter has a good effect on suppressing the baseline drift noise of the ECG signal in the sleep scene.

For some patients suffering from arrhythmia or other heart diseases, we extracted the ECG data of No. 111 from the MIT-BIH Arrhythmia dataset[57] for the experiment, as

shown in Figure 4.9. Comparing the signals before and after filtering, we can find that the baseline of the filtered signals is regular. At the same time, it does not influence the basic morphology of normal beats and arrhythmia-onset beats and retains the main frequency components of normal and abnormal beats.

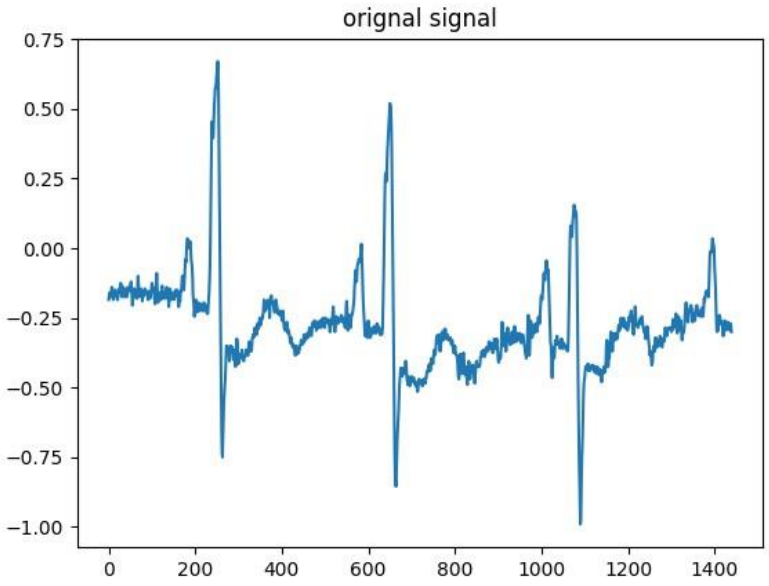

Figure 4.8(a) Fragments of original ECG signals containing arrhythmia.

Figure 4.8(b) Suppression effect of the filter on baseline drift in ECG data containing arrhythmia.

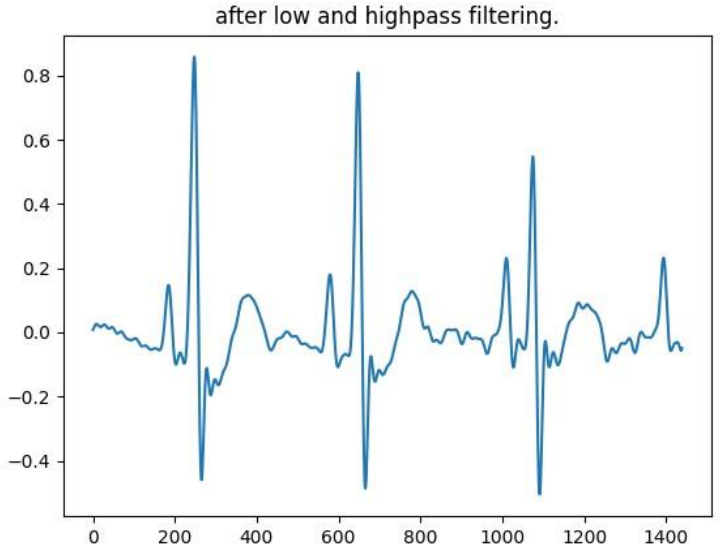

Figure 4.8(c) Fragment of filtered ECG signal containing arrhythmia.

4.2.2 Experimental Results of QRS Wave Group Detection Algorithm

Since the sleep data obtained through our sensors are tests of light sleep and the absence of professional medical guidance, the correctness of the labelling cannot be guaranteed. Therefore, the MIT-BIH Arrhythmia dataset was used to experiment with the QRS detection algorithm. The 48 ECG data from the MIT-BIH Arrhythmia dataset were individually subjected to QRS detection, and the localised QRS wave clusters were compared with the labels provided in the dataset. The QRS wave clusters were considered to have been correctly detected if the error was no more than 30 samples (0.08 seconds).

To quantitatively measure the QRS classification and detection algorithms employed, the performance of the algorithms was quantified by calculating the accuracy (Acc)

$$Acc = \frac{TP}{TP + FN + FP} \times 100\% \tag{4.1}$$

where TP is the number of QRS wave groups that are correctly categorised; FN is the number of QRS wave groups that are not detected; FP is the number of QRS wave groups that are not QRS wave groups but are mistakenly detected as QRS wave groups. Based on the results of the experiments, the accuracy rate is calculated to be 99.79% and the validation accuracy rate is 99.42%.

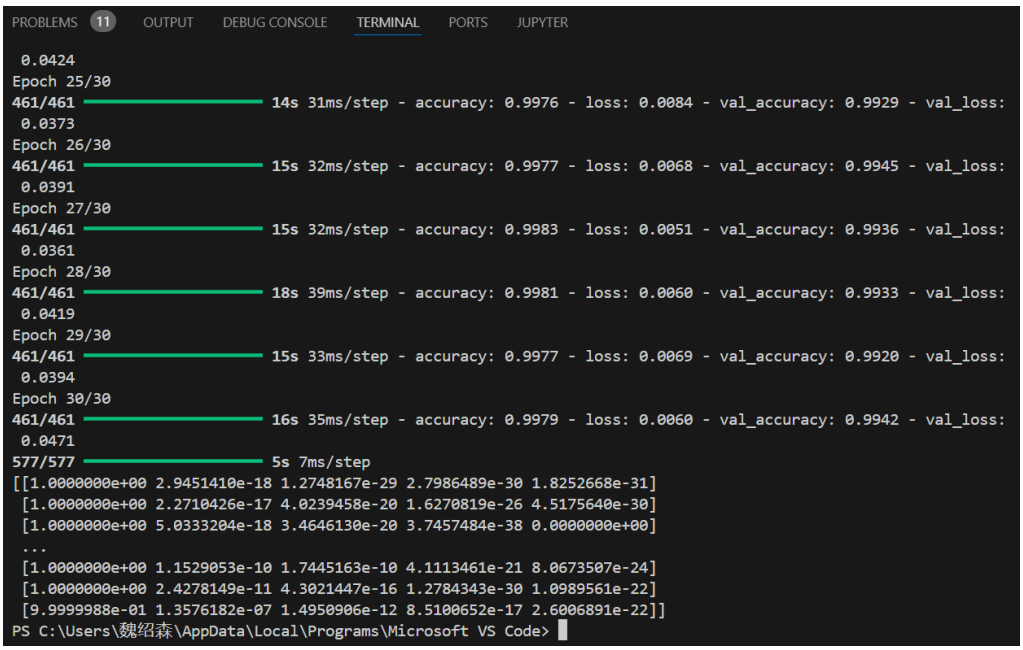

Figure 4.9 Training results

4.3 CONCLUSION

In this chapter, we focus on experimental results regarding self-powered flexible pressure sensors and deep learning-based ECG recognition methods. We first tested the durability and reliability under different environmental conditions to ensure that the sensor was able to detect the pressure sensitivity of subtle pulse signals then did a step-input test to assess the dynamic characteristics as well as a series of volunteer experiments. The results show that the sensor has excellent stability, sensitivity and dynamic responsiveness to effectively detect subtle pulse vibrations. Then, we validated the effectiveness and accuracy of the deep learning method, which mainly used the MIT-BIH arrhythmia dataset to validate the preprocessing and QRS wave cluster detection algorithms, proving its high accuracy and validation rate. In the test of

the CNN-based classification model for ECG recognition, it was able to achieve 98% accuracy in a 7-class classification task.

CHAPTER 5: CONCLUSION

5.1 Significance and Contribution

Sleep apnea has a serious impact on the quality of a patient's sleep due to its characteristic of causing frequent awakenings during sleep. It can affect the patient's mental state and work efficiency during the day and can lead to potential car accidents, as well as cardiovascular disease. Severe cases can even lead to sudden death in sleep

Accidents and cardiovascular diseases are also known as the cause of sleep apnea. Traditionally, sleep apnea diagnosis has relied on PSGs, which are expensive and have complex wires and sensors that can affect the user's sleep. On the other hand, wearable health monitoring devices such as smartwatches are becoming more and more popular with consumers as electronic technology advances and people become more health conscious. Therefore, there is a need to develop a lightweight and low-complexity sleep apnea detection algorithm and a low-power sleep apnea detection system that can be mounted on small and lightweight wearable devices to help users perform sleep monitoring.

The rapid development of materials has led to the development of self-powered soft wearable health detectors, which can be attached to the human skin and utilise the large amount of health-related information and signals contained in the skin for convenient health detection at anytime, anywhere. It is now possible to design PDMS-based pressure sensors that can be triggered by tiny, pulsed vibrations, considering the properties of piezoelectric materials and the current comfortable body-sensor

interaction. In our research practice, we have summarized the many requirements and designed a flexible sandwich structure device using piezoelectric materials with an optimised parallel capacitor configuration. This ultra-thin piezoelectric device has two 4×4 cm^2 silver electrodes with good conductivity coated on the surface of the FEP film on both sides of the sensor. We also tested our silver-coated FEP film (Ag/FEP) and found it to have good charge decay retention. In 200 hours of continuous testing, the initial surface potential of the Ag/FEP layer was about 2000 V. It then continued to drop slowly for the remaining 175 hours, while the surface potential of the PET dropped dramatically to -261 V for 2 hours and then stayed at the same level, suggesting that the sensor can achieve a good self-supply of energy. Double-sided adhesive tape was used to securely bond the four corners of the fluorinated ethylene propylene (FEP) film to form an internal cavity in the ultrathin sensor structure, and the total thickness of the sensor was approximately 300 microns, allowing for amplitude enhancement of the sensor to improve performance.

The sensor operating system we designed is based on the principle of piezoelectricity, where compressing and releasing the device will change the distance of the air gap and the moment of the giant lectric dipole, thus enabling the conversion from mechanical deformation to an electrical signal. We then developed the sleep heartbeat monitoring system by combining an ultra-thin self-powered pressure sensor as a pulse detection sensor, an Arduino board-based circuit and a power supply unit. We tried to use deep learning to enable an end-to-end solution for ECG recognition by eliminating the need for manual filtering and feature extraction, where the ECG data can be sliced and diced into small pieces and fed directly into a model for classification. We used the CNN

network architecture to combine it with Recurrent Neural Network (RNN), and we achieved very high (98%) accuracy for 7 classification tasks.

5.2 Limitations and Potential Issues

For this research, we are facing many challenges, hardware mainly in terms of sensor output enhancement and storage, accurate evaluation of the output, stability, miniaturization, and integration.

In the design process of this project, we mainly focus on the sleep scene of static state, aiming to provide an ideal solution for monitoring of respiratory movement. However, real-life sleep scenarios are often more complex and variable. For example, some people may sleep with their wrists or arms resting on their backs out of habit or for other reasons, while others may roll over or move their bodies violently during sleep. These complex sleep scenarios and forms of movement may cause the accuracy and reliability of the test results to be affected to a certain extent.

In this study, the amount of sleep apnea and electrocardiographic data we used was relatively limited, and we used only 48 strips of annotated ECG data from the PhysioNet MIT-BIH Arrhythmia database and Apnea-ECG database for analysis and modelling. This constrains the generalisability and replicability of the findings.

Another limitation is that the distribution of different categories in these ECG data was not balanced. For example, the number of samples of some abnormal heartbeats may only be one-tenth of the normal heartbeats, resulting in few samples within a class and large differences between classes. This imbalance in data distribution may cause the

model to be biased towards the major classes and neglect the features of the minor classes during training and testing, thus affecting the final classification and detection accuracy.

Since the sample distributions of both the training and testing sets come from the same data source, which does not fully reflect the complex and variable data distributions in real scenarios, the monitoring and classification models developed in this report may encounter performance degradation when they are extended to a wider range of applications.

CHAPTER 6: FUTURE WORK

The hardware system and apnea-arrhythmia detection algorithm proposed in this paper have been improved and optimized in various ways in terms of accuracy and lightness and more impressive results have been achieved. But there are still many aspects that can be further improved.

(1) Clinical data are ever-changing, we should try our best to cooperate with hospitals to get more and more up-to-date sleep clinical data to optimize the algorithm and get better results. In the future, we plan to obtain more comprehensive sleep data from hospitals and other institutions to have more understanding of physiological mechanisms and build more accurate monitoring and prediction models with the support of a larger amount of data. The expansion of data volume will be an important part of our research work.

(2) Since we failed to consider the complexities during the initial design fully, the program still has some limitations in application scenarios. It can only work best in relatively static and standardised sleep environments and can hardly fully adapt to a variety of variable real sleep situations. This also provides a direction for our future improvement and iteration, i.e., we need to carry out in-depth research and optimisation for complex sleep scenarios and movement forms, to achieve high-precision and high-robustness sleep respiration and movement monitoring in a wider range of applications.

(3) During the experiment it was not considered whether different types of clothing and different binding methods to the clothing would have an effect on the results, and therefore only considered on roughly connecting the sensor to the circuit to the clothing. In the future, we should consider the comfort of the user and make it easier for the user to fall asleep.

(4) Although the convolutional neural network-based sleep apnea detection scheme has shown significant improvement in detection performance compared to other traditional machine learning methods, the classification performance needs to be further improved relative to the goal of applying it to consumer products. In addition, the high computational and storage overheads associated with AI algorithms are a major challenge that needs to be addressed.

REFERENCE

[1] 医学会呼吸分会睡眠呼吸障碍学组, 中国医学装备协会呼吸病学装备技术专业委员会睡眠呼吸设备学组. 成人阻塞性睡眠呼吸暂停高危人群筛查与管理专家共识 [J] . 中华健康管理学杂志, 2022, 16(8) : 520-528. DOI: 10.3760/cma.j.cn115624-20220615-00460.

[2] 《中国心血管健康与疾病报告2022》编写组. (2023).《中国心血管健康与疾病报告2022》概述. 中国心血管病研究, 21(7), 577–600. https://doi.org/10.3969/j.issn.1672-5301.2023.07.001

[3] Ciołek M, Niedźwiecki M, Sieklicki S, et al. Automated detection of sleep apnea and hypopnea events based on robust airflow envelope tracking in the presence of breathing artifacts[J]. IEEE Journal of Biomedical and Health Informatics, 2014, 19(2): 418-429.

[4] Kohler M, Pitcher A, Blair E, et al. The impact of obstructive sleep apnea on aortic disease in marfan's syndrome[J]. Respiration, 2013, 86(1): 39-44.

[5] 王志人, 王益新. 心电图初学指南[M]. 北京: 科学技术文献出版社, 2005: 63-99.

[6] Graves A, Mohamed A R, Hinton G. Speech recognition with deep recurrent neural networks[C]. 2013 IEEE International Conference on Acoustics Speech and Signal Processing. IEEE, 2013: 6645-6649.

[7] Z. L. Wang, "Triboelectric nanogenerators for self-powered electronics and sensors," Nano Energy, vol. 68, p. 104359, Feb. 2020, doi: 10.1016/j.nanoen.2019.104359.

[8] J. Wang et al., "Recent advances in nanogenerators-based flexible electronics for electromechanical biomonitoring," Nano Today, vol. 39, p. 101157, Aug. 2021, doi: 10.1016/j.nantod.2021.101157.

[9] N. I. Kim, J. H. Jung, J. Chun, and S. W. Kim, "Soft, flexible pressure sensors for pressure monitoring under large hydrostatic pressure and harsh ocean environments," ACS Applied Materials & Interfaces, vol. 15, no. 11, pp. 14347-14357, Mar. 2023, doi: 10.1021/acsami.2c21963.

[10] S. Wang, J. Y. Oh, J. Xu, H. Tran, and Z. Bao, "Skin-inspired electronics: An emerging paradigm," Accounts of Chemical Research, vol. 51, no. 5, pp. 1033-1045, May 2018, doi: 10.1021/acs.accounts.8b00015.

[11] T. R. Ray et al., "Bio-integrated wearable systems: A comprehensive review," Chemical Reviews, vol. 119, no. 8, pp. 5461-5533, Apr. 2019, doi: 10.1021/acs.chemrev.8b00573.

[12] Y. Khan, A. E. Ostfeld, C. M. Lochner, A. Pierre, and A. C. Arias, "Monitoring of vital signs with flexible and wearable medical devices," Advanced Materials, vol. 28, no. 22, pp. 4373-4395, Jun. 2016, doi: 10.1002/adma.201504366.

[13] M. Hailu, G. Nola, J. Cherston, J. Xie, S. Tawfick, and C. M. Schroeder, "Multifunctional microfluidic skin adhesives for wearable biosensors," Advanced Science, vol. 8, no. 5, p. 2003802, Mar. 2021, doi: 10.1002/advs.202003802.

[14] J. Nie, Z. Wang, Z. Ren, S. Li, X. Chen, and Z. L. Wang, "Power generation from the interaction of a liquid droplet and a liquid membrane," Nature Communications, vol. 10, no. 1, pp. 1-9, Dec. 2019, doi: 10.1038/s41467-019-09851-1.

[15] S. Lee, W. Jang, S. Jang, and H. Choi, "Skin-attachable triboelectric auditory sensors for human–machine interfaces," Nano Energy, vol. 91, p. 106636, Jan. 2022, doi: 10.1016/j.nanoen.2021.106636.

[16] Y. Zang, F. Zhang, C. Di, and D. Zhu, "Advances of flexible pressure sensors toward artificial intelligence and health care applications," Materials Horizons, vol. 2, no. 2, pp. 140-156, Apr. 2015, doi: 10.1039/C4MH00147H.

[17] S. Xu et al., "Assembly of micro/nanomaterials into complex, three-dimensional architectures by compressive buckling," Science, vol. 347, no. 6218, pp. 154-159, Jan. 2015, doi: 10.1126/science.1260960.

[18] Y. Gao, L. Yu, J. C. Yeo, and C. T. Lim, "Flexible hybrid sensors for health monitoring: Materials and mechanisms to render wearability," Advanced Materials, vol. 32, no. 15, p. 1902133, Apr. 2020, doi: 10.1002/adma.201902133.

[19] T. Cheng, Y. Zhang, W. Y. Lai, and W. Huang, "Stretchable thin-film electrodes for flexible electronics with high deformability and stretchability," Advanced Materials, vol. 27, no. 22, pp. 3349-3376, Jun. 2015, doi: 10.1002/adma.201405864.

[20] J. Kim et al., "Stretchable silicon nanoribbon electronics for skin prosthesis," Nature Communications, vol. 5, no. 1, pp. 1-11, Dec. 2014, doi: 10.1038/ncomms6747.

[21] D. Son et al., "An integrated self-healable electronic skin system fabricated via dynamic reconstruction of a nanostructured conducting network," Nature Nanotechnology, vol. 13, no. 11, pp. 1057-1065, Nov. 2018, doi: 10.1038/s41565-018-0244-6.

[22] Y. Khan, A. E. Ostfeld, C. M. Lochner, A. Pierre, and A. C. Arias, "Lab-on-skin: A review of flexible and stretchable electronics for wearable health monitoring," Advanced Functional Materials, vol. 27, no. 11, p. 1605165, Mar. 2017, doi: 10.1002/adfm.201605165.

[23] D. H. Kim, R. Ghaffari, N. Lu, and J. A. Rogers, "Flexible and stretchable electronics for biointegrated devices," Annual Review of Biomedical Engineering, vol. 14, pp. 113-128, Aug. 2012, doi: 10.1146/annurev-bioeng-071811-150018.

[24] Z. Ma, D. Kong, L. Pan, and Z. Bao, "Skin-inspired electronics: Emerging semiconductor devices and systems," Journal of Semiconductors, vol. 41, no. 4, p. 041601, Apr. 2020, doi: 10.1088/1674-4926/41/4/041601.

[25] S. Jung, J. Lee, T. Hyeon, M. Lee, and D. H. Kim, "Fabric‐based integrated energy devices for wearable activity monitors," Advanced Materials, vol. 26, no. 36, pp. 6329-6334, Sep. 2014, doi: 10.1002/adma.201402439.

[26] F. R. Fan, L. Lin, G. Zhu, W. Wu, R. Zhang, and Z. L. Wang, "Transparent triboelectric nanogenerators and self-powered pressure sensors based on micropatterned plastic films," Nano Letters, vol. 12, no. 6, pp. 3109-3114, Jun. 2012, doi: 10.1021/nl300988z.

[27] J. Zhong et al., "Self-powered human-interactive transparent nanopaper systems," ACS Nano, vol. 9, no. 7, pp. 7399-7406, Jul. 2015, doi: 10.1021/acsnano.5b02414.

[28] X. Peng et al., "A breathable, biodegradable, antibacterial, and self-powered electronic skin based on all-nanofiber triboelectric nanogenerators," Science Advances, vol. 6, no. 26, p. eaba9624, Jun. 2020, doi: 10.1126/sciadv.aba9624.

[29] Z. L. Wang and J. Song, "Piezoelectric nanogenerators based on zinc oxide nanowire arrays," Science, vol. 312, no. 5771, pp. 242-246, Apr. 2006, doi: 10.1126/science.1124005.

[30] M. Pandey, N. Mohamad, and A. C. Arias, "Flexible nanogenerators for energy harvesting and self-powered electronics," Advanced Energy Materials, vol. 9, no. 45, p. 1902186, Dec. 2019, doi: 10.1002/aenm.201902186.

[31] J. P. Harmon, A. Srivastava, and Z. L. Wang, "Interfacial slippage in flexible triboelectric nanogenerators," Nano Energy, vol. 76, p. 105066, Oct. 2020, doi: 10.1016/j.nanoen.2020.105066.

[32] F. R. Fan, W. Tang, and Z. L. Wang, "Flexible nanogenerators for energy harvesting and self‐powered electronics," Advanced Materials, vol. 28, no. 22, pp. 4283-4305, Jun. 2016, doi: 10.1002/adma.201504299.

[33] Fan J, Yang S, Liu J, et al. A High Accuracy & Ultra-Low Power ECG-Derived Respiration Estimation Processor for Wearable Respiration Monitoring Sensor[J]. Biosensors, 2022, 12(8): 665.

[34] Charlton P H, Birrenkott D A, Bonnici T, et al. Breathing Rate Estimation from the Electrocardiogram and Photoplethysmogram: A Review[J]. IEEE Reviews in Biomedical Engineering, 2017, 11: 2-20.

[35] Varon C, Morales J, Lázaro J, et al. A Comparative Study of ECG-derived Respiration in Ambulatory Monitoring using the Single-lead ECG[J]. Scientific Reports, 2020, 10(1): 1-14.

[36] Yang S, Fan J, Liu J, et al. A High Accuracy & Low Power EDR Estimation Processor for Wearable Devices[C]. 2021 IEEE International Conference on Integrated Circuits, Technologies and Applications (ICTA). IEEE, 2021: 133-134.

[37] Malik J, Devecioglu O C, Kiranyaz S, et al. Real-time Patient-specific ECG Classification by 1D Self-operational Neural Networks[J]. IEEE Transactions on Biomedical Engineering, 2021, 69(5): 1788-1801.

[38] Pan J, Tompkins W J. A real-time QRS Detection Algorithm[J]. IEEE Transactions on Biomedical Engineering, 1985 (3): 230-236.

[39] Peng S, Fan J, Zhu Z. R-peak Detection for ECG Biomedical Monitoring[C]. 2021 IEEE International Conference on Power, Intelligent Computing and Systems (ICPICS). IEEE, 2021: 12-15.

[40] Tekeste T, Saleh H, Mohammad B, et al. A Nano-watt ECG Feature Extraction Engine in 65-nm Technology[J]. IEEE Transactions on Circuits and Systems II: Express Briefs, 2017, 65(8): 1099-1103.

[41] Pan J, Tompkins W J. A real-time QRS Detection Algorithm[J]. IEEE Transactions on Biomedical Engineering, 1985 (3): 230-236.

[42] Nayak C, Saha S K, Kar R, et al. An Efficient and Robust Digital Fractional Order Differentiator Based ECG Pre-processor Design for QRS Detection[J]. IEEE Transactions on Biomedical Circuits and Systems, 2019, 13(4): 682-696.

[43] Kaur A, Agarwal A, Agarwal R, et al. A Novel Thresholding Technique for R-peak Detection in ECG[C]. 2019 Second International Conference on Advanced Computational and Communication Paradigms (ICACCP). IEEE, 2019: 1-4.

[44] Thiamchoo N, Phukpattaranont P. Application of Wavelet Transform and Shannon Energy on R Peak Detection Algorithm[C]. 2016 13th International Conference on Electrical Engineering/Electronics, Computer, Telecommunications and Information Technology (ECTI-CON). IEEE, 2016: 1-5.

[45] Aqil M, Jbari A, Bourouhou A. Adaptive ECG Wavelet Analysis for R-peaks Detection[C]. 2016 International Conference on Electrical and Information Technologies (ICEIT). IEEE, 2016: 164-167.

[46] Manikandan M S, Soman K P. A Novel Method for Detecting R-peaks in Electrocardiogram (ECG) Signal[J]. Biomedical Signal Processing and Control, 2012, 7(2): 118-128.

[47] Somers V K, Dyken M E, Clary M P, et al. Sympathetic Neural Mechanisms in Obstructive Sleep Apnea[J]. The Journal of Clinical Investigation, 1995, 96(4): 1897-1904.

[48] Yeo M, Byun H, Lee J, et al. Respiratory Event Detection During Sleep Using Electrocardiogram and Respiratory Related Signals: Using Polysomnogram and Patch-type Wearable Device Data[J]. IEEE Journal of Biomedical and Health Informatics, 2021, 26(2): 550-560.

[49] Surrel G, Aminifar A, Rincón F, et al. Online Obstructive Sleep Apnea Detection on Medical Wearable Sensors[J]. IEEE Transactions on Biomedical Circuits and Systems, 2018, 12(4): 762-773.

[50] Sheta A, Turabieh H, Thaher T, et al. Diagnosis of Obstructive Sleep Apnea from ECG Signals Using Machine Learning and Deep Learning Classifiers[J]. Applied Sciences, 2021, 11(14): 6622.

[51] Redmon J, Divvala S, Girshick R, et al. You Only Look Once: Unified, Real-time Object Detection[C]. Proceedings of the IEEE Conference on Computer Vision and Pattern Recognition. 2016: 779-788.

[52] 王涛, 鲁昌华, 孙怡宁, 等. 多尺度卷积神经网络检测睡眠呼吸暂停[J]. 电子测量与仪器学报, 2021, 35(07): 30-35.

[53] Rajabrundha A, Lakshmisangeetha, Balajiganesh A. Analysis of Sleep apnea Considering Electrocardiogram Data Using Deep Learning Algorithms[C]. Journal of Physics: Conference Series. IOP Publishing, 2022, 2318(1): 012009.

[54] Sharan, Roneel & Berkovsky, Shlomo & Xiong, Hao & Coiera, Enrico. (2020). ECG-derived heart rate variability interpolation and 1-D convolutional neural networks for detecting sleep apnea. 2020. 637-640. 10.1109/EMBC44109.2020.9175998.

[55] Nguyen, Anh-Tu & Nguyen, Thao & Le, Huy-Khiem & Pham, Hieu & Do, Cuong. (2022). A novel deep learning-based approach for sleep apnea detection using single-lead ECG signals. 2046-2052. 10.23919/APSIPAASC55919.2022.9979890.

[56] Zhong, J., Ma, Y., Song, Y., Zhong, Q., Chu, Y., Karakurt, I., Bogy, D. B., & Lin, L. (2019). A Flexible Piezoelectret Actuator/Sensor Patch for Mechanical Human-Machine Interfaces. ACS nano, 13(6), 7107–7116. https://doi.org/10.1021/acsnano.9b02437

[57] Moody GB, Mark RG. The impact of the MIT-BIH Arrhythmia Database. IEEE Eng in Med and Biol 20(3):45-50 (May-June 2001). (PMID: 11446209)

[58] Goldberger, A., Amaral, L., Glass, L., Hausdorff, J., Ivanov, P. C., Mark, R., ... & Stanley, H. E. (2000). PhysioBank, PhysioToolkit, and PhysioNet: Components of a new research resource for complex physiologic signals. Circulation [Online]. 101 (23), pp. e215–e220.

[59] Penzel T, Moody G B, Mark R G, et al. The apnea-ECG database[C]. Computers in Cardiology 2000. IEEE, 2000: 255-258.

[60] Zidelmal Z, Amirou A, Adnane M, et al. QRS detection based on wavelet coefficients[J]. Computer Methods and Programs in Biomedicine, 2012, 107(03): 490-496

[61] Kohler B U, Hennig C, Orglmeister R. The principles of software QRS detection[J]. IEEE Engineering in Medicine and biology Magazine, 2002, 21(1): 42-57

[62] Hamilton, P S, Tompkins, W J. Quantitative investigation of QRS detection rules using the MIT/BIH arrhythmia database[J]. IEEE Transactions on Bio Medical Engineering, 1986, 33(12): 1157-1165.

[63] Acharya, U. R., Oh, S. L., Hagiwara, Y., Tan, J. H., Adam, M., Gertych, A., & Tan, R. S. (2017). A deep convolutional neural network model to classify heartbeats. Computers in Biology and Medicine, 89, 389–396. https://doi.org/10.1016/j.compbiomed.2017.08.022

APPENDIX A: SUPPORTING INFORMATION

Supplementary Figures and Tables

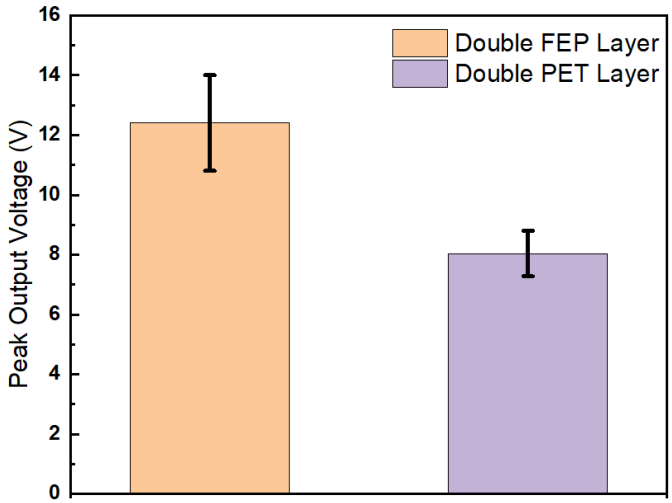

Figure S1. Test results of peak output voltage between double FEP layer and double PET layer.

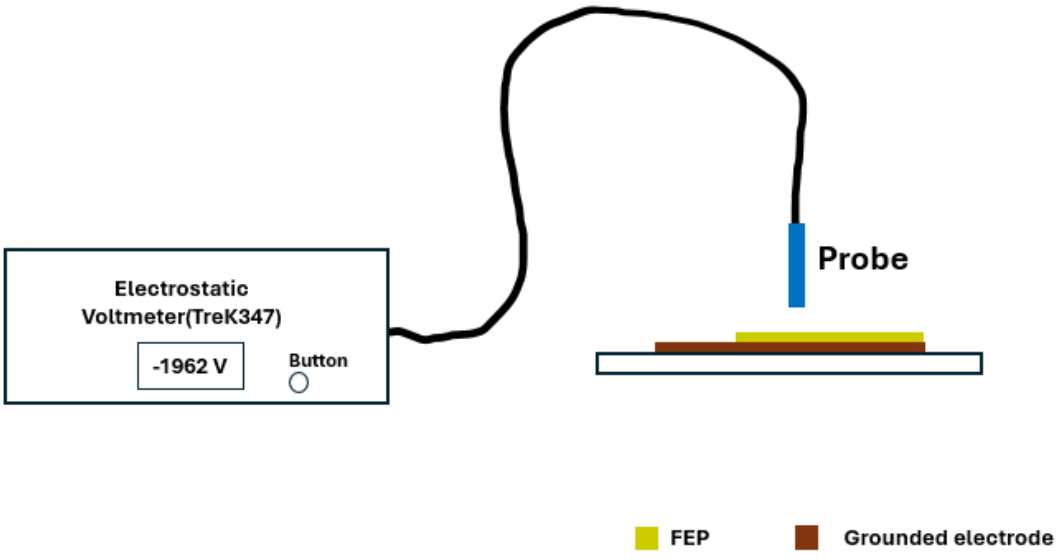

Figure S2. Schematic diagram of measuring method for FEP layer

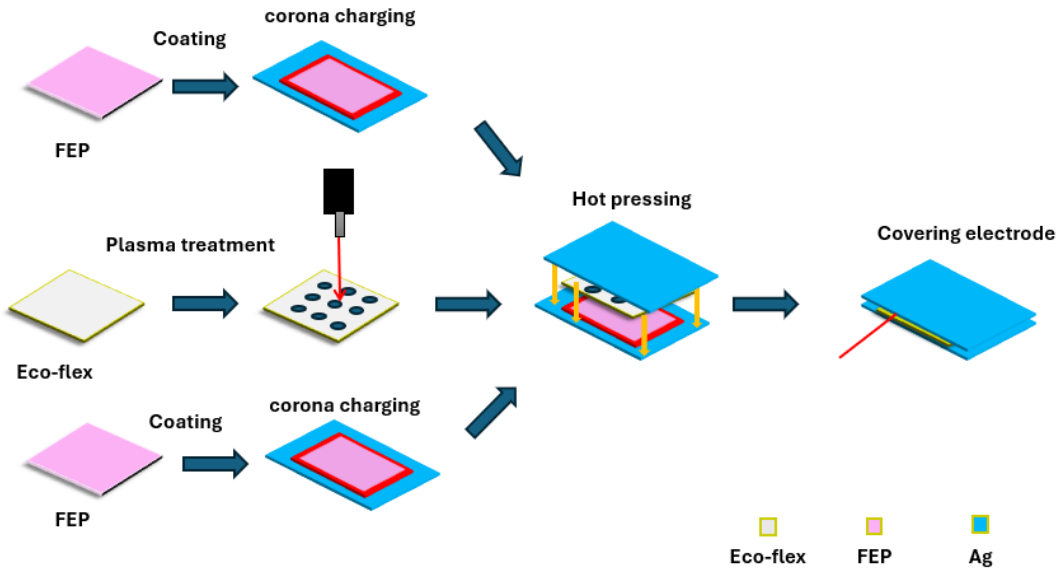

Figure S3. Schematic diagram illustrating the fabrication steps of the self-powered flexible sensor.

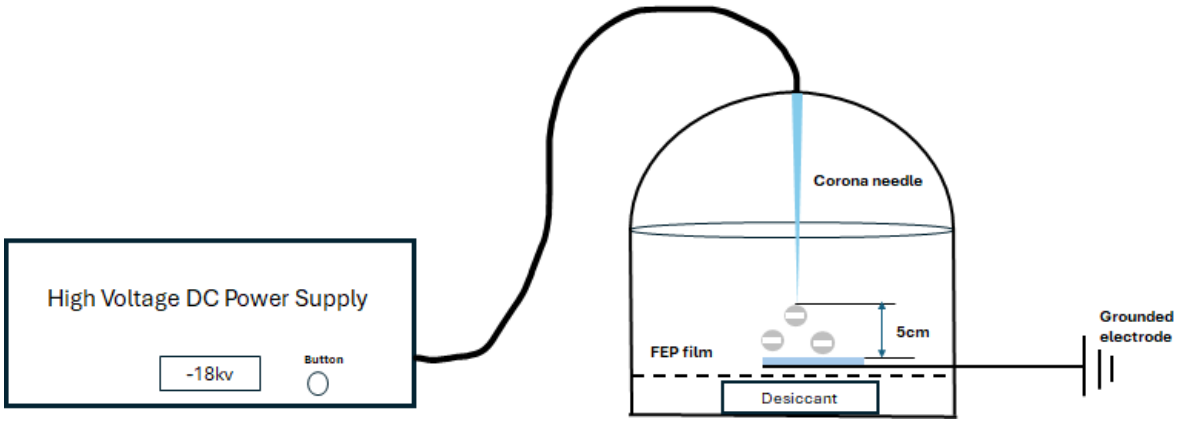

Figure S4. Schematic diagram of the corona charging device. Samples were placed 5cm below the needle tip for about 5 min. The high voltage applied to the needle tip is about -18 kV.

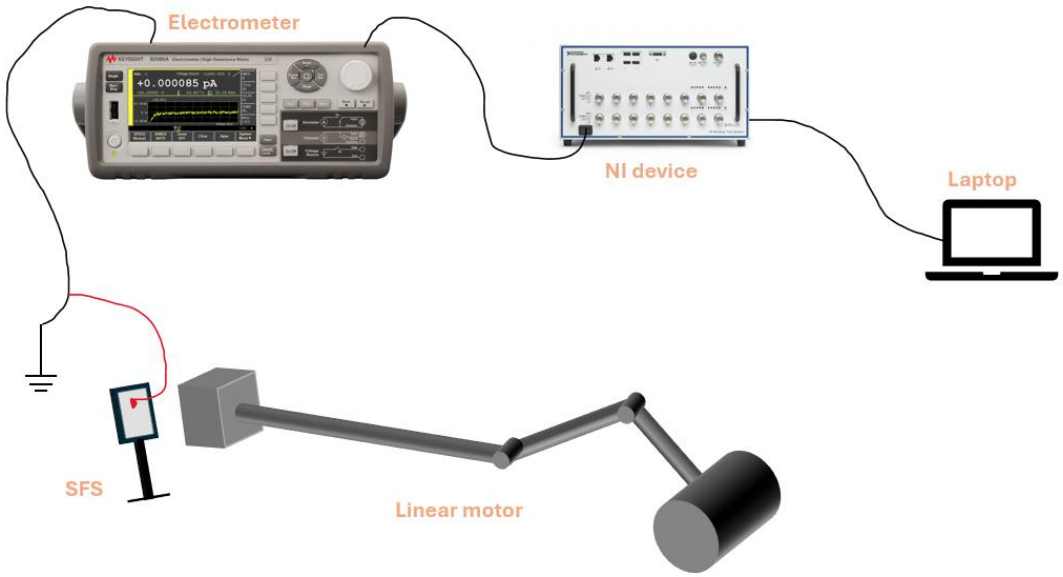

Figure S5. Schematic diagram illustrating the electrical connections between the SFS, electrometer, and NI data acquisition system.

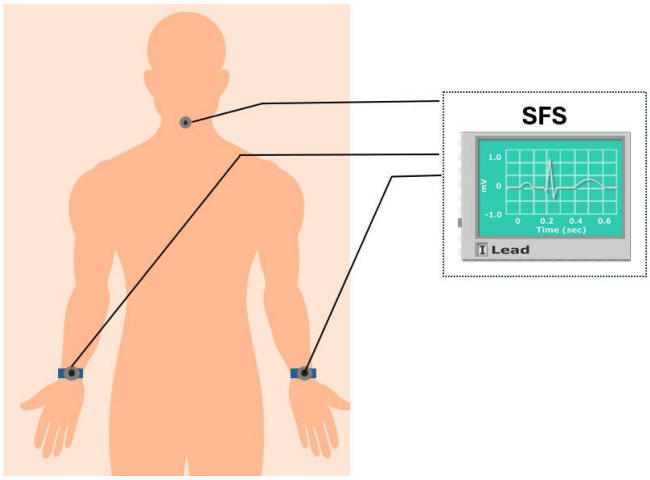

Figure S6. Schematic diagram demonstrating the application scenario

SAS Class	**AHI (times /h)**
Mild	5≤AHI<15
Moderate	15≤AHI<30
Severe	AHI≥30

Table S1. SAS classification basis

APPENDIX B: CODE EXAMPLES

Data Preprocessing

```
import os
import shutil
import pandas as pd
import wfdb
import numpy as np
import matplotlib.pyplot as plt
from sklearn import preprocessing
import pywt
from scipy import signal

mit_bih_dir = r'C:\Users\魏绍森\AppData\Local\Programs\Microsoft VS
Code\mit-bih-arrhythmia-database-1.0.0'
mit_bih_dest = r'C:\Users\魏绍森\AppData\Local\Programs\Microsoft VS
Code\mit-bih-arrhythmia-database-p-wave-annotations-1.0.0'

# Categories of heartbeats in the MIT-BIH database based on AAMI.
heartbeat_classes = [
('N', ['N','L','R','e','j']), # normal category
('S', ['A','a','J','S']), # Supraventricular ectopic
('V', ['V','E']), # Ventricular ectopic
('F', ['F']), # Fusion
('Q', ['/','f','Q','r','B','n','?']) # Unknown category (any other beats)
]

# known beat classes
known_classes = np.array(['N','S','V','F','Q'])

#combined dataset
DS = [ '101', '106', '108', '109', '112', '114', '115', '116', '118', '119', '122', '124',
'201', '203', '205', '207',
        '208', '209', '215', '220', '223', '230', '100', '103', '105', '111', '113',
'117', '121', '123', '200', '202', '210',
        '212', '213', '214', '219', '221', '222', '228', '231', '232', '233', '234']



def normalize(data):
```

```
    data = np.nan_to_num(data)  # removing NaNs and Infs
    data = preprocessing.minmax_scale(p_signal, feature_range=(0, 1), axis=0,
copy=True)
    return data


def ecg_denoise(ecg,symbol):

    ##
    #remove baselinewander
    ##
    data = []
    for i in range(len(ecg) - 1):
        Y = ecg[i]
        Y = Y.astype(float)
        data.append(Y)

    # Create wavelet object and define parameters
    w = pywt.Wavelet('db5')  # Daubechies8

    # Decompose into wavelet components, to the level selected:
    coeffs = pywt.wavedec(data, 'db8', level=8)  # The signal is decomposed by wavelet

    #wavelet reconstruction
    bw_denoised = pywt.waverec(np.multiply(coeffs, [0, 1, 1, 1, 1,1,1,1,1]).tolist(),
'db8')  # The signal is reconstructed by wavelet

    #detect R-Wave
    # read annatations
    plt.figure()
    plt.plot(ecg[258840:260280])
    plt.title("orignal signal")

    plt.figure()
    plt.plot(bw_denoised[258840:260280])
    plt.title("after basewander removal")

    ##
    #Remove baselinewander
    ##
    b, a = signal.butter(8, 0.1, 'lowpass')   #set filter;8 order
    ecg_1 = signal.filtfilt(b, a, bw_denoised)  #dbw_denoise need to be removed
    b, a = signal.butter(8, 0.007, 'highpass')
    denoised_ecg = signal.filtfilt(b, a,ecg_1 )
```

```
    plt.figure()
    plt.plot(denoised_ecg[258840:260280])
    plt.title("after low and highpass filtering.")

    plt.show()

    return denoised_ecg



classes = {'F': 0, 'N': 1, 'Q': 2, 'S': 3, 'V': 4}

# convert label characters to number representation
def char_to_num(data):

    # print(np.unique(data), "unique classes")
    # print(data.shape, "before char to num")

    for cl in classes:
       data = [classes[cl] if sym == cl else sym for sym in data] #replace symbols with
number representations

    data = np.array(data, dtype=np.int32)

    # print(np.unique(data), "unique classes")
    # print(data.shape, "after char to num")

    return data

# encodes labels using one-hot encoding
def labels_to_one_hot(labels, dimension=5):
    results = np.zeros((len(labels), dimension), dtype=np.int32)
    for i , label in enumerate(labels):
        results[i, label] = 1
    return results


ds_dir = 'intra'

save_dir = os.path.join(mit_bih_dest,ds_dir+'/')

if os.path.exists(save_dir): # delete directory if exists
    shutil.rmtree(save_dir)
os.makedirs(save_dir)
```

```
## points left and right of the Rpeak
Rpeak_left = 103
Rpeak_right = 247

beat_length = Rpeak_left + Rpeak_right
total_samples = 100733 #got after a test run

# preallocate array size
sample_count = 0
x_samples = np.array(total_samples*[beat_length*[0.0]])  #initialize empty array for
beats
y_labels = np.array(total_samples*[None]) # initialize empty array for beat labels

for record_name in DS:

    fname = os.path.join(mit_bih_dir, str(record_name)) # creating file name

    try:  # if some numbers don't exist in the records
        annotation = wfdb.rdann(fname, 'atr')
        record = wfdb.rdrecord(fname)
    except:
        continue

    symbols = np.array(annotation.symbol)
    samples = np.array(annotation.sample)
    p_signal = record.p_signal    # extract signal
    ## extract lead two channel
    if record_name == "114": #this record has inverted channels
        p_signal = p_signal[:,1] # MLII
    else:
        p_signal = p_signal[:,0] # MLII

    denoised = ecg_denoise(p_signal, symbols)
    p_signal = denoised

    # test plot
    # plt.plot(p_signal[63315-5000:63315+500,0])
    # plt.show()

    for cat,syms in heartbeat_classes:  # loop over categories
        for s in syms: # loop through the symbols
            ndx = np.nonzero(symbols == s)[0]
            if ndx.size: # indice array isn't empty
```

```
                symbols[ndx] = cat

    # label, total = np.unique(symbols, return_counts=True)
    # print(label, total)

    # normalize between 0 and 1
    p_signal = normalize(p_signal)

    # loop over beat annotations
    i = 0
    for sym in symbols:
        if sym in known_classes: # symbol is in known category

            # find beat start
            beat_start = samples[i] - Rpeak_left
            left_pad = 0
            if beat_start < 0:
                left_pad = -beat_start
                beat_start = 0

            # find beat end
            beat_end = samples[i] + Rpeak_right
            right_pad = 0
            if beat_end > p_signal.size:
                right_pad = beat_end - p_signal.size
                beat_end = p_signal.size

            # grab single beat
            single_beat = p_signal[beat_start:beat_end]
            single_beat = np.pad(single_beat,(left_pad,
right_pad),mode='edge')

            # # append to beat array
            # if x_samples.size == 0: # first beat
            #     x_samples = np.array(single_beat)
            #     y_labels = np.array(sym)
            # else:
            #     # x_samples = np.vstack((x_samples,single_beat))
            #     y_labels = np.append(y_labels,sym)

            # insert samples into array
            y_labels[sample_count] = sym
            x_samples[sample_count][:] = single_beat
            sample_count = sample_count + 1
```

```
            #print(x_samples.shape, y_labels.shape)

            #print((i, sym, samples[i]))
            # plt.plot(x_samples[sample_count-1][:])
            # #plt.show()
            # plt.title('i is'+str(i))
            # plt.pause(0.001)


        i = i + 1 # increment i
    print(record_name)

y_labels = labels_to_one_hot(char_to_num(y_labels))
print(y_labels)

# save samples and labels
np.save(os.path.join(save_dir,'beat_samples'), x_samples)
np.save(os.path.join(save_dir,'beat_labels'), y_labels)
```

Training Codes

```
import sys
sys.path.insert(0, r'C:\Users\魏绍森\AppData\Local\Programs\Microsoft VS Code')

import os
from matplotlib.cbook import flatten
import pandas as pd
import wfdb
import matplotlib.pyplot as plt
import numpy as np
import math
import operator
import pydot as pydot
import graphviz

from sklearn.model_selection import train_test_split
from keras import models
from keras import layers
from keras.utils  import plot_model

# force use CPU instead of GPU
os.environ["CUDA_DEVICE_ORDER"] = "PCI_BUS_ID"   # see issue #152
os.environ["CUDA_VISIBLE_DEVICES"] = ""
```

```
# path to the test and train datasets
mit_bih_dir = r'C:\Users\魏绍森\AppData\Local\Programs\Microsoft VS
Code\mit-bih-arrhythmia-database-1.0.0'

labels_file = mit_bih_dir+"/beat_labels.npy"
samples_file = mit_bih_dir+"/beat_samples.npy"

data = np.load(samples_file,allow_pickle=True)
targets = np.load(labels_file,allow_pickle=True)

# train test split
train_data, test_data, train_targets, test_targets = train_test_split(data, targets,
test_size=0.33,shuffle=True)

#train validation split
train_data, val_data, train_targets, val_targets = train_test_split(train_data,
train_targets, test_size=0.2,shuffle=True)

classes = {'F': 0, 'N': 1, 'Q': 2, 'S': 3, 'V': 4}

# test data statistics
label_total = test_targets.sum(axis=0)

label_total = [(c, classes[c]) for c in classes]

print("test data statistics", label_total)

# plt.figure()
# plt.plot(train_data[100])
# plt.show()
# plt.figure()

# training globals
num_epochs = 150

# building the network
def build_model(input_shape):
    model = models.Sequential()

    # model.add(layers.Dense(200, activation='tanh',
    #                        input_shape=(input_shape,)))
    # model.add(layers.Dense(50, activation='tanh'))
    # # end with a softmax layer with 5 units since we have 5 classes to predict
    # model.add(layers.Dense(5, activation='softmax'))
```

```
    print('input_shape', input_shape)

    model.add(layers.Conv1D(52, 15, activation='relu', input_shape=(input_shape,1,)))
    model.add(layers.MaxPooling1D(96, 1))
    model.add(layers.Conv1D(16, 15, activation='relu'))
    model.add(layers.MaxPooling1D(44, 1))
    model.add(layers.Conv1D(8, 6, activation='relu'))
    model.add(layers.MaxPooling1D(19, 1))
    model.add(layers.Flatten())

    # end with a softmax layer with 5 units since we have 5 classes to predict
    model.add(layers.Dense(5, activation='softmax'))
    model.compile(optimizer='rmsprop',
                  loss='categorical_crossentropy',
                  metrics=['acc'])
    return model

# print(np.unique(partial_train_targets), "about to build")
model = build_model(train_data.shape[1])

print(model.summary()) #print model summary

plot_model(model,"cnn_intra_model.png")

history = model.fit(
    train_data,
    train_targets,
    epochs=num_epochs,
    batch_size=1024,
    verbose=1,
    validation_data=(val_data, val_targets)
    )

model.save('ecg_5cat_intra_cnn_classification.h5')

training_loss_history = history.history['loss']
validation_loss_history = history.history['val_loss']

# evaluation of training
epochs = range(1, len(training_loss_history)+1)

plt.plot(epochs, training_loss_history, 'bo', label='Training loss')
plt.plot(epochs, validation_loss_history, 'b', label='Validation loss')
plt.title('Training and validation loss')
plt.xlabel('Epochs')
```

```
plt.ylabel('Loss')
plt.legend()

plt.show()

# model evaluation
results = model.evaluate(test_data, test_targets)
print(f"accuracy on test data:{results[1]}")

# prediction
predictions = model.predict(test_data)

# print(predictions[0])

index_max, value_max = max(enumerate(predictions[0]), key=operator.itemgetter(1))

title = "beat is class: "
i = 0
for key in classes:
    if(i == index_max):
        title = title+key+" confidence: "+str(value_max)+"actual class is
"+str(test_targets[0])
        break
    i = i+1

single_beat = test_data[0]
plt.plot(single_beat)
plt.title(title)
plt.show()

import pywt
import seaborn
import tensorflow as tf
from sklearn.metrics import confusion_matrix

# The proportion of the test set in the data set
RATIO = 0.2

# Wavelet denoising preprocessing
def denoise(data):
    # wavelet transformation
    coeffs = pywt.wavedec(data=data, wavelet='db5', level=9)
    cA9, cD9, cD8, cD7, cD6, cD5, cD4, cD3, cD2, cD1 = coeffs
    # threshold de-noising
    threshold = (np.median(np.abs(cD1)) / 0.6745) * (np.sqrt(2 * np.log(len(cD1))))
```

```
    cD1.fill(0)
    cD2.fill(0)
    for i in range(1, len(coeffs) - 2):
        coeffs[i] = pywt.threshold(coeffs[i], threshold)
    rdata = pywt.waverec(coeffs=coeffs, wavelet='db5')
    return rdata

# Ecg data and corresponding labels are read, and the data is denoised by wavelet
def getDataSet(number, X_data, Y_data):
    ecgClassSet = ['N', 'A', 'V', 'L', 'R']

    record = wfdb.rdrecord('C:/Users/魏绍森/AppData/Local/Programs/Microsoft VS
Code/mit-bih-arrhythmia-database-1.0.0/' + number, channel_names=['MLII'])
    data = record.p_signal.flatten()
    rdata = denoise(data=data)

    annotation = wfdb.rdann('C:/Users/魏绍森/AppData/Local/Programs/Microsoft VS
Code/mit-bih-arrhythmia-database-1.0.0/' + number, 'atr')
    Rlocation = annotation.sample
    Rclass = annotation.symbol
    # Remove the unstable data before and after
    start = 10
    end = 5
    i = start
    j = len(annotation.symbol) - end
   # only the five NAVLR ECG types are selected, select the data required in this record
with a specific label and discard the remaining labeled points
    # X_data Data points of length 300 are intercepted before and after the R wave
    # Y_data Converts NAVLR to 01234 in sequence
    while i < j:
        try:
            # Rclass[i] label
            lable = ecgClassSet.index(Rclass[i])
         # Based on the experience value, take 100 points forward and 200 points backward
based on the R-peak
            x_train = rdata[Rlocation[i] - 100:Rlocation[i] + 200]
            X_data.append(x_train)
            Y_data.append(lable)
            i += 1
        except ValueError:
            i += 1
    return
def loadData():
    numberSet = ['100', '101', '103', '105', '106', '107', '108', '109', '111', '112',
'113', '114', '115',
```

```
                '116', '117', '119', '121', '122', '123', '124', '200', '201', '202',
'203', '205', '208',
                '210', '212', '213', '214', '215', '217', '219', '220', '221', '222',
'223', '228', '230',
                '231', '232', '233', '234']
    dataSet = []
    lableSet = []
    for n in numberSet:
        getDataSet(n, dataSet, lableSet)
    # Turn the numpy array, out of order
    dataSet = np.array(dataSet).reshape(-1, 300)
    lableSet = np.array(lableSet).reshape(-1, 1)
    train_ds = np.hstack((dataSet, lableSet))
    np.random.shuffle(train_ds)
    # Data set and its label set
    X = train_ds[:, :300].reshape(-1, 300, 1)
    Y = train_ds[:, 300]
    # Test set and its tag set
    shuffle_index = np.random.permutation(len(X))
    # set initial value, RATIO is the proportion of the test set in the data set
    test_length = int(RATIO * len(shuffle_index))
    # The length of the test set
    test_index = shuffle_index[:test_length]
    # The length of the train set
    train_index = shuffle_index[test_length:]
    X_test, Y_test = X[test_index], Y[test_index]
    X_train, Y_train = X[train_index], Y[train_index]
    return X_train, Y_train, X_test, Y_test

# Construct CNN model
def buildModel():
    newModel = tf.keras.models.Sequential([
        tf.keras.layers.InputLayer(input_shape=(300, 1)),
        # The first convolution layer, four 21x1 convolution cores
        tf.keras.layers.Conv1D(filters=4, kernel_size=21, strides=1, padding='same',
activation='tanh'),
        #First pooled layer, maximum pooled,4 3x1 convolution nuclei, step size 2
        tf.keras.layers.MaxPool1D(pool_size=3, strides=2, padding='same'),
        # The second convolution layer, 16 23x1 convolution cores
       tf.keras.layers.Conv1D(filters=16, kernel_size=23, strides=1, padding='same',
activation='relu'),
       # The second pooled layer, the maximum pooled, has four 3x1 convolution nuclei
with step size 2
        tf.keras.layers.MaxPool1D(pool_size=3, strides=2, padding='same'),
        # The third convolution layer, 32 25x1 convolution cores
```

```
        tf.keras.layers.Conv1D(filters=32, kernel_size=25, strides=1, padding='same',
activation='tanh'),
       # The third pooling layer, average pooling, has four 3x1 convolution nuclei with
step size 2
        tf.keras.layers.AvgPool1D(pool_size=3, strides=2, padding='same'),
        # The fourth convolution layer, 64 27x1 convolution cores
        tf.keras.layers.Conv1D(filters=64, kernel_size=27, strides=1, padding='same',
activation='relu'),
        # Flat layer, easy to fully connected layer processing
        tf.keras.layers.Flatten(),
        # At the full connection layer,128 nodes are converted to 128 nodes
        tf.keras.layers.Dense(128, activation='relu'),
        # Dropout layer,dropout = 0.2
        tf.keras.layers.Dropout(rate=0.2),
        # Fully connected layer,5 nodes
        tf.keras.layers.Dense(5, activation='softmax')
    ])
    return newModel

def plotHeatMap(Y_test, Y_pred):
    con_mat = confusion_matrix(Y_test, Y_pred)
    # draw
    plt.figure(figsize=(4, 5))
    seaborn.heatmap(con_mat, annot=True, fmt='.20g', cmap='Blues')
    plt.ylim(0, 5)
    plt.xlabel('Predicted labels')
    plt.ylabel('True labels')
    plt.show()


def main():
    # X_train,Y_trai For all data sets and tag sets
    # X_test,Y_test
    X_train, Y_train, X_test, Y_test = loadData()
    print(X_train.shape)

    model = buildModel()
    model.compile(optimizer='adam',
                  loss='sparse_categorical_crossentropy', metrics=['accuracy']
                  # metrics
                  )
    model.summary()

    # training & validation
```

```
    model.fit(X_train, Y_train, epochs=30, batch_size=128, validation_split=RATIO)  #
validation_split The proportion of training sets
    # prediction
    Y_pred = model.predict(X_test)
    print(Y_pred)

if __name__ == '__main__':
    main()
```

APPENDIX C: WORK BREAKDOWN